# Climatic Controls of Fire in the Western United States: From the Atmosphere to Ecosystems

by

S.W. Hostetler[1], P.J. Bartlein[2], A.M. Solomon[3], J.O. Holman[1], R.T. Busing[1,3], and S.L. Shafer[1]

Final report for project 01-1-6-05
Submitted to the Joint Fire Sciences Program
December, 2005

[1]U.S. Geological Survey, Corvallis, Oregon, [2]Department of Geography, University of Oregon, Eugene, Oregon, [3]US Environmental Protection Agency, Corvallis, Oregon

## *Introduction*

The dependence of wildfire on current and antecedent weather conditions is relatively well understood (Rothermel, 1972; Brown and Bevins, 1986; Pyne et al., 1996, Ch. 4; Goens and Ferguson, 2000), and this understanding forms the basis of hourly to weekly prediction of fire behavior. In contrast, relations between climate (i.e., monthly to multi-annual variations of atmospheric circulation) and fire are less well understood, although that understanding is improving (e.g., Westerling et al., 2003).

We believe a better understanding of climate-fire relations would provide a context for fully informed forecasts of fire weather. Our research therefore focused on decomposing and quantifying the hierarchy of climatic controls that influence surface climate conditions prior to and during the fire season in the western United States. To achieve our goal, we employed an approach in which we examined jointly 1) observational (and simulated, or "reanalysis") records of climate and 2) historical records of fire using data-analytical procedures employed in climate-diagnostic studies and a hierarchy of appropriate regional climate and vegetation models.

We were able to quantify climate fire relations, evaluate scaling issues associated with the use of atmospheric models in fire research, and initiate research aimed at linking long-term climate variations to ecosystem responses with the goal of understanding the potential role of climate in natural restoration and reduction of fuel loading.

Here we present an overview of our analysis of fire-climate relations in the Western US on decadal, annual, monthly, and daily time scales. For our analysis, we rely primarily on the 1980-2000 monthly fire-start and area-burned data set of Westerling et al. (2003), the 1986-1996 daily fire start and area burned data of Hardy et al. (2001), observed precipitation and air temperature data (Mitchell et al. 2003), the NOAA/NCEP reanalysis data (Kistler et al. 2001), and an extensive set of climate data produced for this project with a regional climate model, RegCM2 (Giorgi et al., 1993).

A key product of our JFSP-funded research was development of an atlas of climate-fire relationships in the Western US. Our atlas of monthly fire-climate analyses for each of 8 regions of the West is included in a separate file.

Another central effort in this project was production of a 1950-2005 (to date) simulation of weather and climate with our regional climate model. We applied the regional model because it simulates atmospheric and surface fields at temporal and spatial scales that are more applicable in fire-climate research than are those of general circulation climate models. Extensive recoding and model testing were required to modify the regional model so that it could be driven by boundary conditions that were derived from the NCEP reanlaysis fields.

## *Data*

### *Monthly fire data*

The 1980-2000 monthly Westerling et al. (2003) fire data set (Fig. 1) is based on ~300,000 fire reports of fire starts and area burned from the USFS, BLM, NPS, and BIA. The fire reports were assessed for data quality, combined, and interpolated onto a 1° × 1° grid covering 31° to 49° north latitude and 101°-125°W longitude.

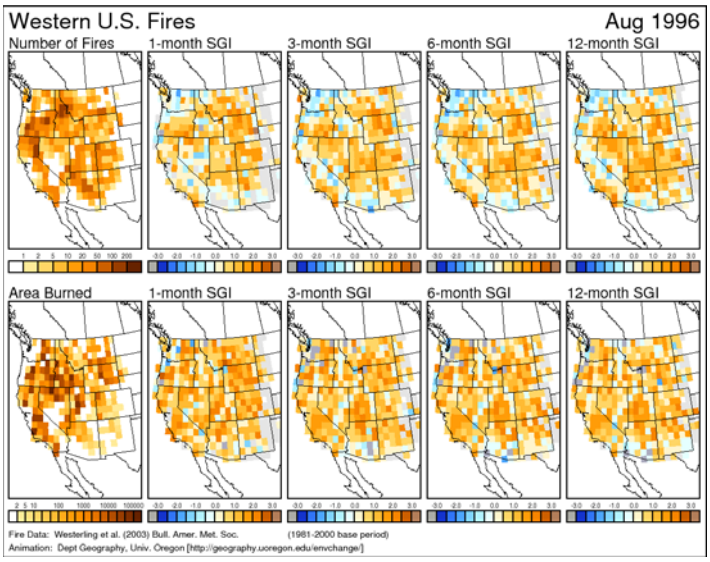


**Figure 1**. Example of the Westerling et al. (2003) wildfire data for August, 1996.

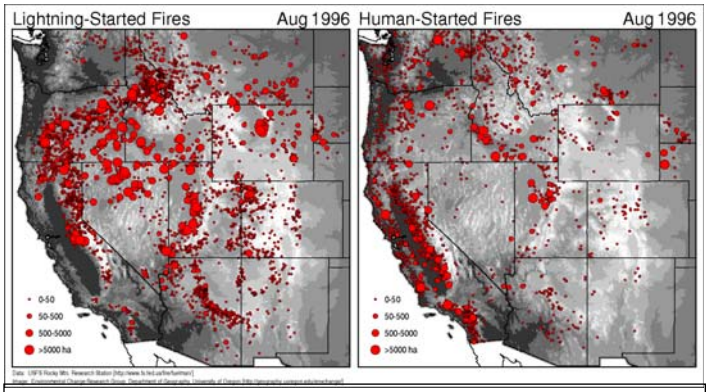


**Figure 2**. Example of the Hardy et al. (2001) daily fire data for August, 1996. Red dots are scaled in size to indicate area burned at a given location. The data set consist of the number and total area of fires on a 1-degree grid, which we used to calculate standardized gamma indices over 1, 3, 6, and 12-month intervals.

### *Daily fire data*

We used the 1986-1996 National Fire Occurrence Database as described in Hardy et al. (2001) and Schmidt et al. (2002), is available at http://www.fs.fed.us/fire/fuelman/. These data consist of records of the locations of individual fires (Fig. 2), the date when each fire was first reported and, for most records, the ultimate size and the date when the fire was considered to have been controlled (but not necessarily extinguished). A subset of the full data set was ex-

tracted containing 332,404 records, including 116,489 fires started by lightning and 197,617 fires started by humans west of 102°W (the region depicted in Fig. 2). These data are not without problems, and thus the raw data set and believe that they are sufficient for our purposes. Further discussion of the nature of these daily fire-start records is provided by Hardy et al. (2001), the review by Westerling et al. (2003), and in an assessment of the quality of such point-location data by Brown et al. (2002).

### *Climate Research Unit (CRU) monthly data*

Monthly observed temperature and precipitation fields (Fig. 3) were described using the "CRU TS 2.0" data set (Mitchell et al. 2003), a global, 0.5-degree gridded data set (for land points only), that spans the interval 1901-2000. We used this data set because it allowed us to calculate "long-term" means for the specific interval represented by the fire data (1980-2000), and because the interpolation inherent in its creation provides data for regions of the western US where individual climate stations are sparse.

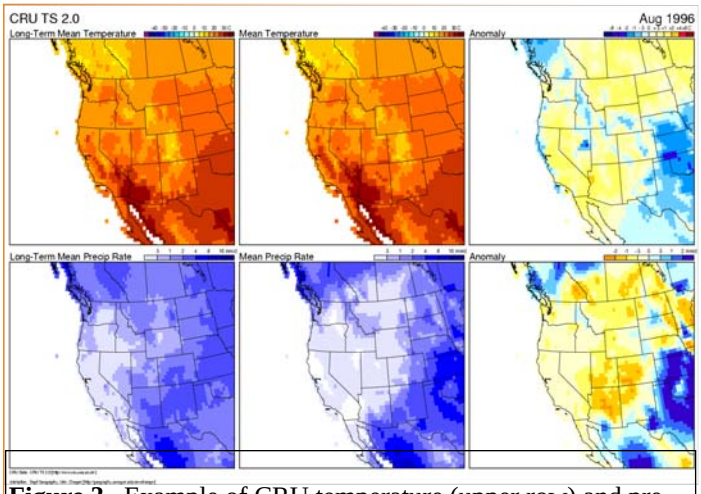


**Figure 3**. Example of CRU temperature (upper row) and precipitation (lower row) for August, 1996.

### *Regional climate model hourly-monthly data*

Global atmospheric and surface climate fields for the period 1948-2005 (through November) have been produced by the NOAA National Center for Environmental Prediction (NCEP) using a sophisticated assimilation technique to incorporate a large number of observed data sets (e.g., atmospheric soundings, sea-surface temperature) into a global atmospheric model (Kistler et al. 2001). The NCEP model has a nominal horizontal grid spacing of 2.5 degrees (about 250 km on a side) and is capable of simulating large-scale synoptic climate features and regional climate variations. The relatively coarse spatial scale of the model, however, limits the degree to which regional climate details are resolved over the topographically complex region of Western North America (Fig. 4).

To provide access to higher resolution climate data, we have produced a continuous, high resolution (45 km horizontal grid, ~0.4 degree) simulation for the period 1950-2005 (to date) using our modified version of the NCAR

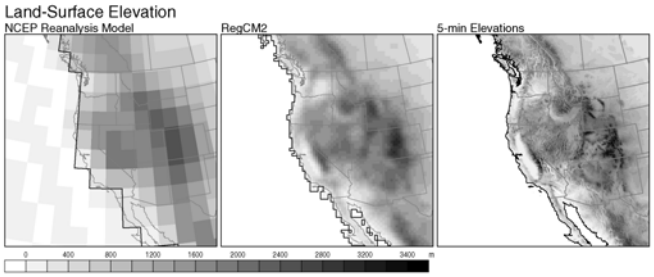


**Figure 4**. Representation of the topography of western North America in A: the NCEP AGCM, B: the RegCM, C: 5-minute DEM. (From Hostetler et al., 2003)

RegCM2 regional climate model (Giorgi et al., 1993) that was designed for this project. The RegCM is derived from the NCAR MM4 meteorological model and is thus also related to the NCAR MM5 model. The RegCM simulation is driven by temporally varying lateral (vertical profiles of temperature, wind, humidity) and surface (pressure and sea surface temperature) boundary conditions derived from the 6-hr NCEP reanalysis history files. A 150-sec model time step was used for the RegCM simulations, which allowed archiving hourly values of the model fields for analysis and plotting. A full year of raw model output files is about 50 Gb in size so the entire 54-year data set is approximately 2.7 Tb.

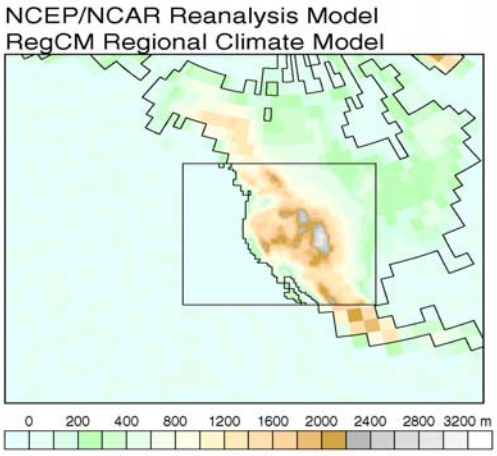


**Figure 5**. RegCM topography inset within the topography as represented by the NCEP GCM. The difference in model resolution of the topography is indicative of similar differences in the resolution of atmospheric and surface fields.

The RegCM domain covers the western U.S. and adjacent areas of Canada and Mexico; there are 3510 terrestrial grid points (Figs. 4, 5). At 45-km grid spacing climatically important physiographic features such as coastlines and the basin and range topography that dominates the West are resolved (Figs. 4, 5).

Our configuration of the RegCM is fully coupled at the boundary layer with a sophisticated land-surface model, LSX (Land Surface Exchange model, Thompson and Pollard, 1995), that computes the exchange of energy and mass based on specified vegetation and soil properties. LSX

includes a 6-layer, dynamic soil model that calculates soil temperature and the frozen and liquid water content in the top 4.5m of the soil.

To achieve quality simulations with the RegCM it is necessary to optimize the coupling between the forcing NCEP GCM large-scale boundary conditions and the RegCM. We focused considerable effort on the coupling with satisfactory results. The quality of the coupling between the NCEP and RegCM models is illustrated in Fig. 6 and 7. Together, the atmospheric models provide internally consistent climate information from the surface to the upper atmosphere

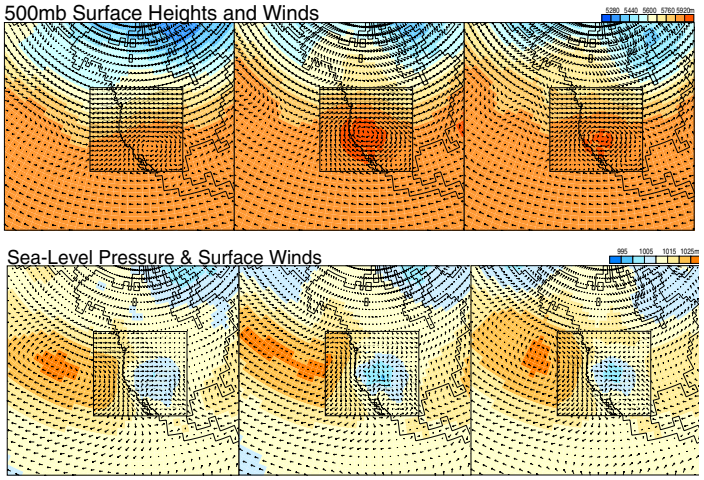


**Figure 6**. 500 hPa height and wind vectors and sea level pressure and wind vectors. The larger area of the Northern hemisphere shows the 500 hPa and SLP fields for the NCEP model. The 500 hPa and SLP fields for the RegCM are plotted in the smaller rectangle which is the spatial domain of the RegCM. The uniformity of the features in the model along the RegCM boundary indicates how well the NCEP boundary conditions are introduced into the RegCM.

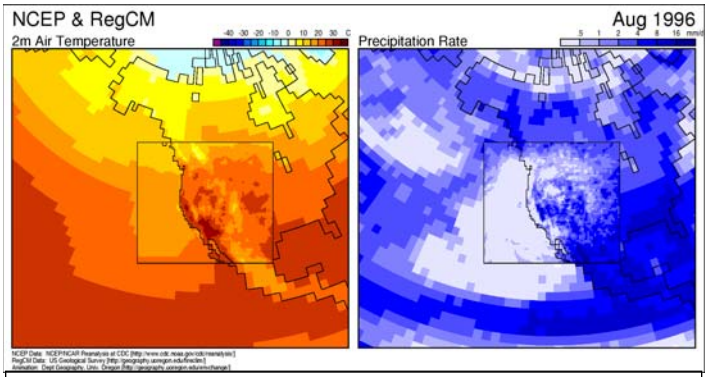


**Figure 7**. Examples of 2-m air temperature and precipitation as simulated by the RegCM for August, 1996. The RegCM domain is shown inside the larger NCEP model domain. All simulated RegCM atmospheric and surface fields are available for each grid point in the domain.

over a wide range of spatial scales and on temporal scales ranging from hourly to decades.

## *The nature of wildfire in the West*

### *Decadal fire occurrence*

The 20th-century fire record of area burned for the Western US (Fig. 8) displays considerable inter-annual to decadal variability. From 1920 through the mid-1940s antiphasing of fire size is apparent between the Northwest and Southwest. From the late 1940s through the 1980s, the regions were more-or-less in phase with diminished

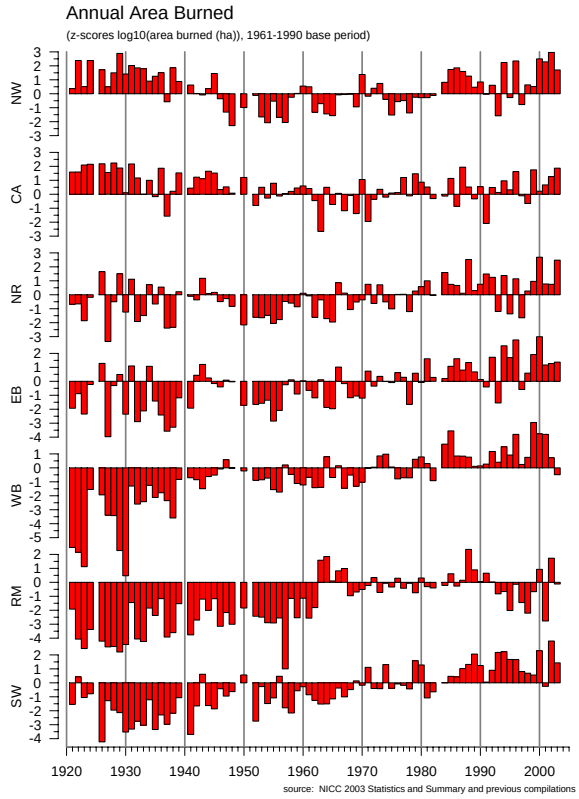


**Figure 8**. 1920-2003 total area burned by wildfires in the Western US. NW: Northwest, CA: California, NR: Northern Rocky Mountains; EB: Eastern Great Basin, WB: Western Great Basin, RM: Central Rocky Mountains, SW: Southwest. Data compiled from various federal agencies.

variability. After the 1980s, variability increased with no obvious indication of synchrony. The fire record implicitly includes the effects of increasing fire suppression and the ecology of managed and unmanaged wildlands. As we will show, however, the record also clearly displays climatic-derived mediation from annual, multi-annual, and decadal climatic variations.

### *Annual and seasonal fire occurrence*

The annual and seasonal patterns of lightning and human caused wildfires (Fig. 9) are broadly associated with the major topographically and climatically determined Bailey ecoregions (Fig. 10). Wildfire from both ignition sources display an underlying reliance on climate, but the climatic and meteorologic influence on a particular fire season or run of fire seasons is expressed stronger for lightning-caused fires. Fire outbreaks occur earliest in the dry desert and semi-desert regions of the Southwest and Northwest

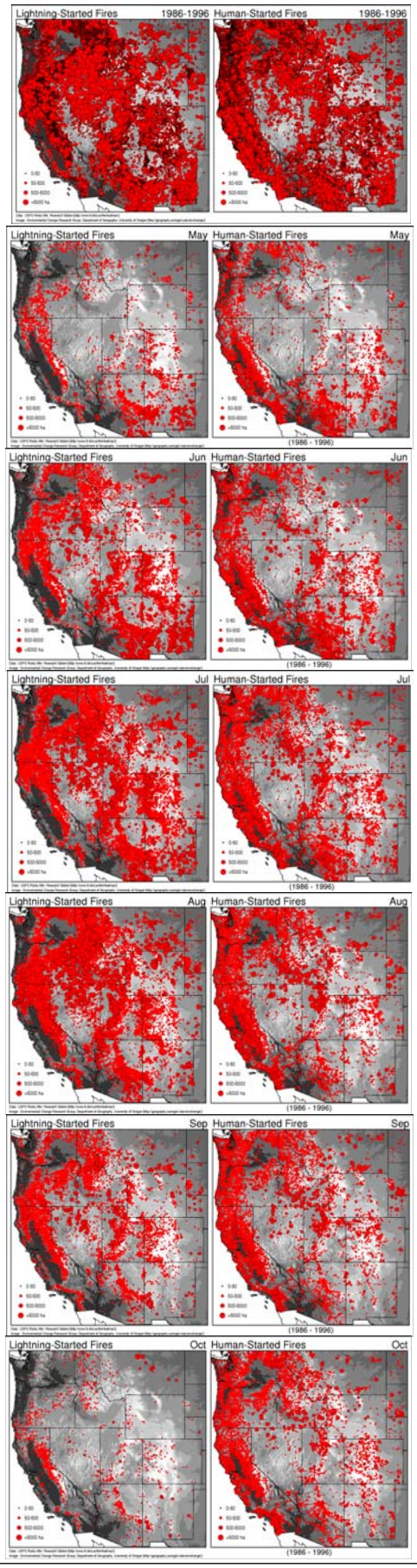


**Figure 9**. 1986-1996 annual and May-October area burned for lightning (left column) and human-started (right column) wildfires.

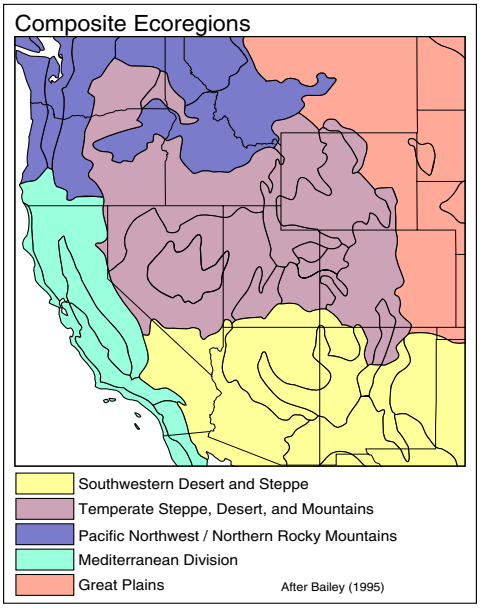


**Figure 10**. The five Bailey composite ecoregions of the Western US. From Bartlein et al (2003).

and in the dry areas of Northern California and eastern slope of the Sierra Nevada. Fire outbreaks intensify in these regions and progress into the other regions. After the summer peak, fall fire outbreaks are similar to those of the spring. The general pattern of the seasonal cycle of wildfire is evident in all years of the fire record, but the density and timing of the fires for a given season is strongly controlled by prevailing antecedent and contemporaneous climate and weather conditions.

### *Daily fire occurrence*

The total number of fires from all ignition sources for each day of the year, plotted as a function of day number (Fig. 11), resembles a Gaussian curve that reaches an annual maximum during the first half of August. Fires started by lightning are almost entirely restricted to the interval from late April through October, while those started by human causes occur during any month of the year. There is a prominent singularity in the frequency of human-started fires around the Fourth of July, when daily fire frequencies attain levels three times higher than those just before or after the holiday. High summertime levels of human-started fires tend to taper off gradually during the autumn, with a slight shoulder in the distribution marking the end of the summer outdoor-recreation season at the end of October. In general, the shape of the distribution of the total number of fires resembles that of the lightning-started fires more than that of the human-started fires; the latter act mainly to determine the shape of the distribution of all fires during the late autumn, winter, and early spring. Despite the large number of human-started fires, the variation in the total number of fires during the summer is strongly modulated by the number of lightning-started fires.

The time of year of peak incidence of fires from all sources varies both across the western U.S. and among the ecoregions (Fig. 12). Fires occur earlier in the southwestern desert and steppe composite ecoregions (SW), and progress, in order, into the intermountain west and southern Rocky

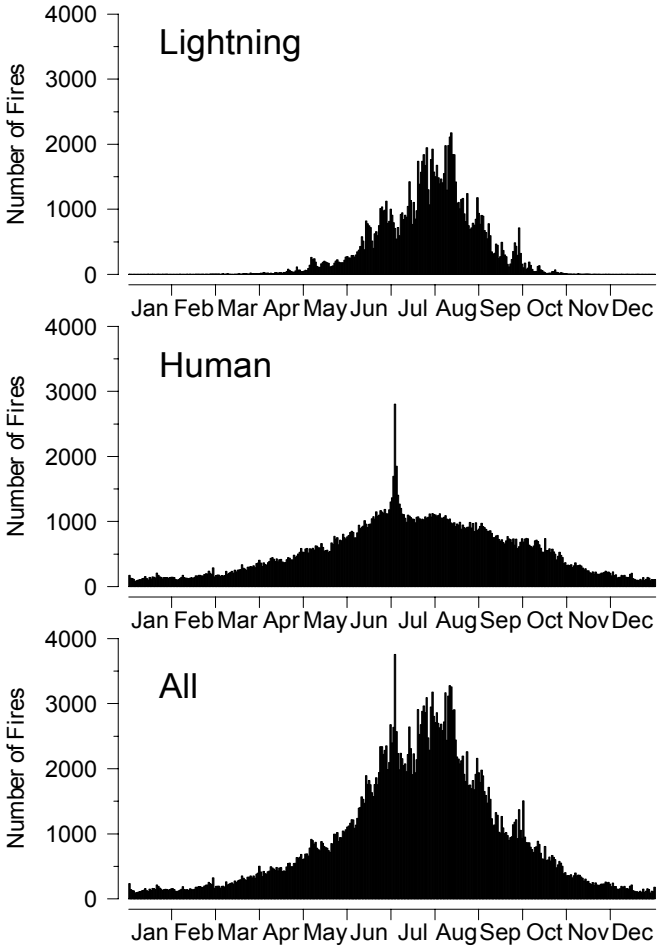


**Figure 11**. Annual distribution of daily fire starts for the period 1986-1996.

Mountains (the Temperate Steppe, Desert and Mountains composite ecoregion (TSDM)), the Pacific Northwest and northern Rocky Mountains (PNW & NRM), and California (i.e. the Mediterranean Division (MD) composite ecoregion). Wintertime fires in the western U.S. are almost exclusively

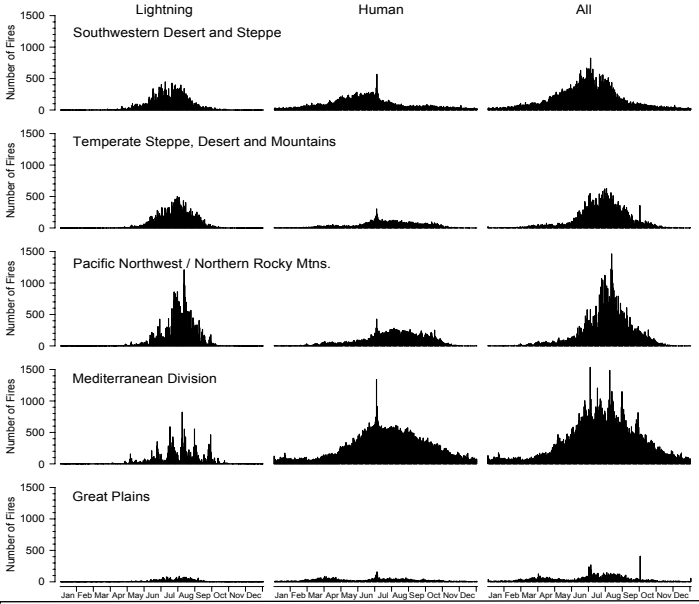


**Figure 12**. Distributions of 1986-1996 daily fire starts within each Bailey composite ecoregion.

restricted to the MD region. Human-started fires in the MD region and increase in number earlier in the year than in the PNW & NRM region, reflecting the generally drier conditions and larger populations there.

With the exception of the Mediterranean Division (MD), the timing of the peak number of human-started fires and fires from all sources follow the progression of lightning-started fires. (The very small number of fires in the Great Plains (GP) composite ecoregion is an artifact of the fire-reporting process for non-federal lands (Westerling et al. 2003; Brown et al. 2002), and represents severe underreporting of fires there.)

In addition to standard time series plots and maps, we also analyzed the fire data using time-space plots, known to climatologists as Hovmöller diagrams (Hovmöller 1949). In their application here, the Hovmöller diagrams take the form of scatter diagrams with space (location) plotted along the x-axis and time (in days during the 11-year interval 1986-1996) plotted along the y-axis, with individual fires plotted as points.

The Hovmöller diagrams illustrate the greater number of human-started fires relative to lightning-started ones in the western U.S. The seasonal cycles of each ignition source are also apparent. By noting the location of the lines demarcating 1 July for each year, it is clear that lightning-started fires occur primarily in spring and summer with fewer fires occurring during the fall and winter. In contrast, the human-started fires plot as much broader clouds of points indicating more continuous fire occurrence throughout the year. The overall shape of the annual clouds of lightning-started fires decline slightly from right to left on the diagrams and reflect the earlier beginning of the lightning-started fire season in the southeastern part of the region.

Lightning-started fires occur in prominent horizontal streaks of points (separated by clear gaps between the streaks) that illustrate widespread fire outbreaks across the region (and intervening periods with few lightning-started fires). In contrast, the prominent streaks in the human-started fires diagram are oriented vertically, and thus represent multiple ignitions that occurred at specific locations over the course of the year. The primary controls underlying the patterns evident in the lightning-started fires diagram are therefore clearly weather- and climate-related, whereas the underlying control of human-started fires is location and consequently related to the intensity of human activity in a particular area.

The streaks on the lightning-started fires diagram suggests that most of these widespread fire outbreaks are time-transgressive, inasmuch as they occur first in the western part of the region, and progress within a few days to the eastern part, reflecting the eastward migration of the controlling weather systems. Many of the horizontal streaks in these data span a relatively large longitudinal distance, as do the gaps between the outbreaks, which together imply region-wide coherence in fire-related meteorological conditions.

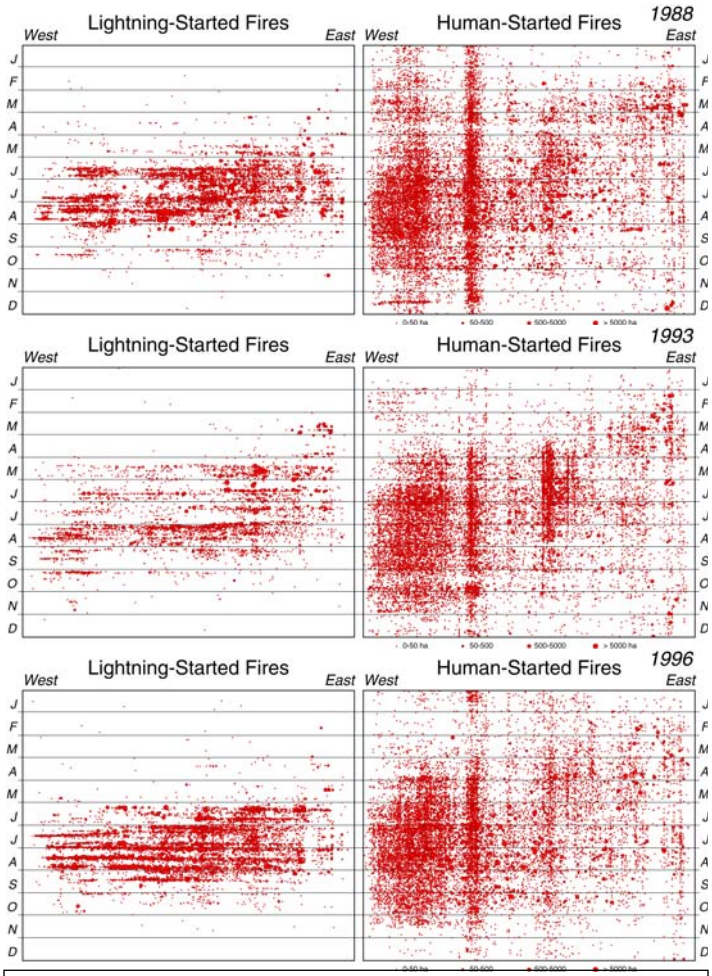


**Figure 13**. Hovmöller diagrams of daily fire starts for 1988, 1993, and 1996.

## *Fire and Climate data analysis*

Although we have analyzed many potential variables from our regional climate model simulations, the subset we use here summarizes the main features of climate that are needed to isolate and identify fire-climate interactions in the West on a daily and monthly time scale. We include data for the Southern Oscillation index (ENSO) which has been suggested as a candidate index in many climate-wildfire investigations.

### *Data transformations*

For many fire-climate analyses, we transformed the raw fire (i.e., area burned and number of fires) or climate (e.g. precipitation) data into "standardized gamma indices" using the mathematical algorithms for computing the standardized precipitation index (SPI, McKee et al., 1993; Hays et al., 1996; Edwards and McKee, 1997; Guttman, 1998, 1999). The SPI was developed as a methods for describing long-term precipitation anomalies and drought indicators in a way that allows comparisons to be made across different climate regions among which the underlying statistical distributions precipitation may vary widely, e.g. from negative-exponential distributions with many zeros to Gaussian-like symmetric distributions.

The SPI is calculated by fitting a gamma distribution to the raw data, calculating gamma CDF-ordinate (i.e. probability) values for those data, and then calculating Gaussian (normal) PDF-abscissa values for these. The computed standardized gamma value (SGI, or SPI in the case of precipitation) is thus a number with values that range between -3 and +3 that can be interpreted as standardized deviations from the long-term mean for a particular month or season (or z-scores). The SGI thereby transforms the data onto a common scale that is independent of the data type, underlying distributions, and units of a particular variable, allowing direct comparison and correlation among variables.

Another desirable strength of the SI method lies in the ease with which index values spanning runs of months (e.g., over 1, 6, 12, 24, 48 months) can be computed. We focus here on time periods of 1, 3, 6, and 12 months. The 1-month index is simply a measure, in standard deviations, of how much the given month departs from the average of all other like months (e.g. how much the August, 1988 fire frequency departs from the average of all August fire frequencies in the record). The 3-month index indicates how much a given three-month period, e.g., June, July, August, 1988, departs from the average of all other June-August periods in the record, and so on. The family of indices thus underpins a straightforward approach for investigating how fire behavior depends on a range of contemporaneous and antecedent climatic conditions.

### *Historical fire-climate relations*

Some degree of success has been achieved in associating past fire seasons with various phases of multi year to decadal climate oscillations such as ENSO and PDO

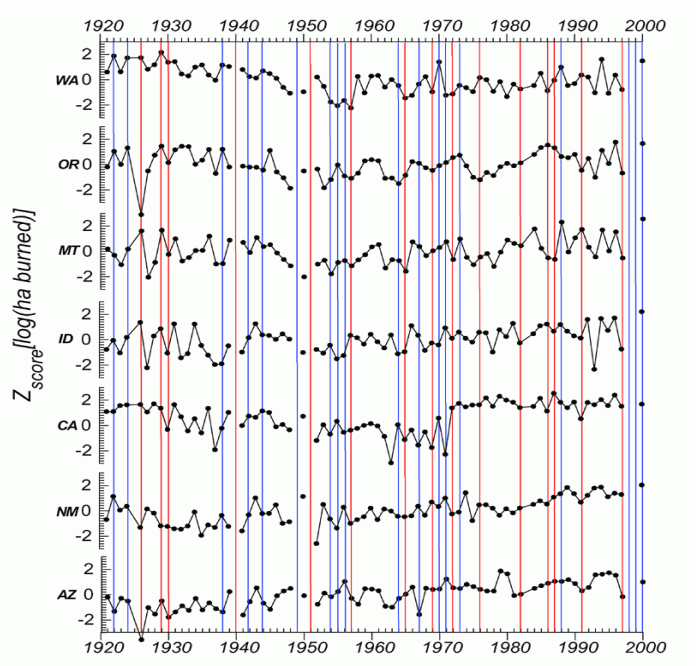


**Figure 14**. Area burned over the last century and phase of the Southern Oscillation Index. Red lines are El Nino (warm events) and blue lines are La Nina (cold events). Data compiled from Federal and State agency reports.

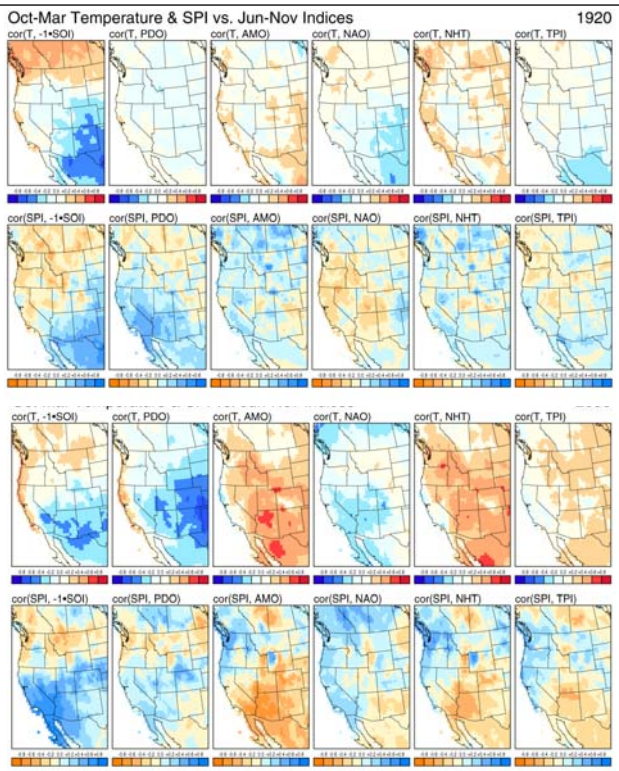


**Figure 15**. Correlations between temperature and precipitation in the Western US and selected climate modes. Indices are: Southern Oscillation Index (SOI, multiplied by -1.0), the Pacific Decadal Oscillation (PDO), the Atlantic Multidecadal Oscillation (AMO), the North Atlantic Oscillation (NAO), northern hemisphere mean temperature (NHT), and the Trans-Polar Index (TPI, the pressure difference between Hobart, Australia and Stanley, Falkland Is.

(Simard et al., 1985; Flannigan et al., 2000; Westerling et al., 2001). Correlations with climate indices such as ENSO and PDO are only partly successful, however, because both high, low, and normal fire years in the historical record have occurred during the various phases of these events (Fig. 14). Moreover, correlations between most modes of climate variability and surface fields such as temperature and precipitation are nonstationary and so change through time (Fig. 15) across sub-regions of the West (McCabe and Dettinger, 1999; Cole and Cook, 1998; Gershunov and Barnett, 1998). In some cases, even the sign of the correlation has changed over decades.

A recent example of possible problems encountered in correlating these indices with fire conditions occurred during the 2000 fire season. The presence of a persistent La Niña was forecast to bring wetter than normal conditions to the Pacific Northwest and Northern Rocky Mountains; however, precipitation in these areas actually ranged from normal to below normal. The inconsistency of the 2000 winter precipitation with expected patterns points to the general problem of directly associating fire conditions with circulation indices such as ENSO and PDO. While underlying relations between fire conditions and these indices exist, the apparent weakness of the correlation and the possibility of multiple climatic-determined controls of fire underscores what we believe is a fundamental issue in fire science: a lack of understanding of the relation among the temporal and spatial characteristics of atmospheric circulation (climate versus weather) and fire conditions.

The role of interannual climatic variations in influencing large-region area-burned variations (Fig. 16, on the page 10) is illustrated using seasonal temperature and precipitation anomalies calculated using the CRU 0.5-degree gridded monthly climate data set. Temperature anomalies are actual deviations from the 1971-2000 averages; precipitation anomalies are expressed using the standardized precipitation index. The same base period was used to calculate the SPI, and the values plotted are "3-month" SPI values. The area-burned data (shown in Fig. 8) was compiled from several heterogeneous data sources and, particularly during the interval prior to 1960, is subject to considerable uncertainty. Despite this uncertainty, even during the first part of this record, there is a good correlation with climate data, suggesting that the overall trends in the area-burned data that have usually been ascribed to fire suppression are mediated by 20th-Century climate variations.

Years with large areas burned (Fig. 16, upper four map sets) are characterized by variable temperature anomalies, but with a general tendency for positive anomalies to occur at times during the period from April to September. In contrast, SPI values are generally highly negative particularly for the June-August interval. (In other comparisons, the 3- and 6-month SPI values show the strongest relationships to areas burned). Years with low areas burned are characterized by negative temperature anomalies during the interval from April through August, and positive SPI values, particularly in the June-August interval.

Soil moisture variations throughout the year reflect the trade off between moisture supply from precipitation and snowmelt, and evaporative demand, driven by net radiation and hence ultimately by insolation. As an integrator of the moisture and energy balances, soil moisture anomalies of dry and wet periods are spatially and temporally consistent with both the number and severity of fires over the fire-prone regions of the US (Fig.17, page 11).

### *Seasonal cycle of climate variable*s

The seasonal cycles of various climate variables in the western US reflect the direct effects of insolation on surface water and energy balances, along with the indirect effects of insolation on atmospheric circulation, and hence precipitation. The seasonal cycle of temperature (Fig. 18, page 12) clearly expresses the insolation effect, but also illustrates the thermal inertia of the oceans and their influence on terrestrial climate. Monthly mean temperatures peak in July (and in some locations, August), after the summer solstice, and intermonthly changes in temperature are greatest in the continental interior, and least along the west coast. The effects of elevation on temperature are clearly apparent throughout the year: month-to-month increases in temperature in spring in high-elevation areas remain relatively small until winter snowpack has melted.

The seasonal cycle of precipitation reflects the anti-phasing of two dominant atmospheric circulation features that are driven by the seasonal cycle of insolation. The first mechanism, the midlatitude westerlies, are strongest and farthest south during the winter, when the latitudinal temperature gradient is steepest and the circumpolar vortex is at its greatest extent. Storm systems frequently form in the Gulf of Alaska in winter and move onshore, providing support for precipitation derived ultimately from moisture from subtropical Pacific sources. Precipitation is greatest in winter along the west coast, and in higher-elevation areas in the interior, where it accumulates in winter snow pack. From winter into spring and summer, the westerlies retreat poleward as the temperature gradient is diminished, so that in summer (June, July, and August), westerly-derived precipitation is confined to Canada.

The second precipitation mechanism is the southwestern or Mexican monsoon, which is driven by differential heating of the continent and ocean in the summer. This differential heating generates low pressure over the continent, high pressure over the oceans, and consequent onshore flow of subtropical-Pacific moisture into the southern and southeastern part of the region, from May through August (Fig. 18). A second monsoon-like surge of moisture from the Gulf of Mexico in spring is evident along the eastern edge of the region mapped in Fig. 18. The interplay between these two circulation systems generates patterns in

## High fire years

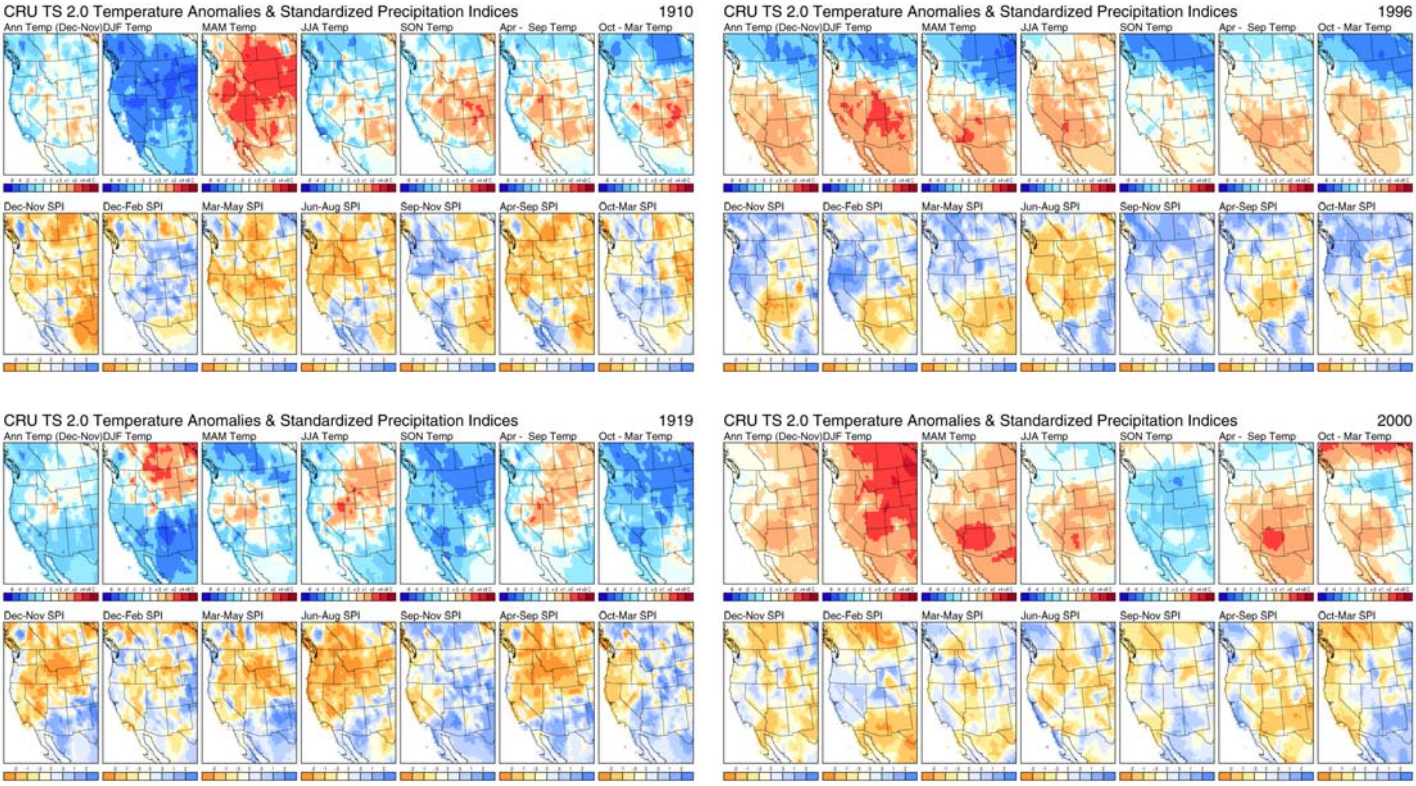


## Low fire years

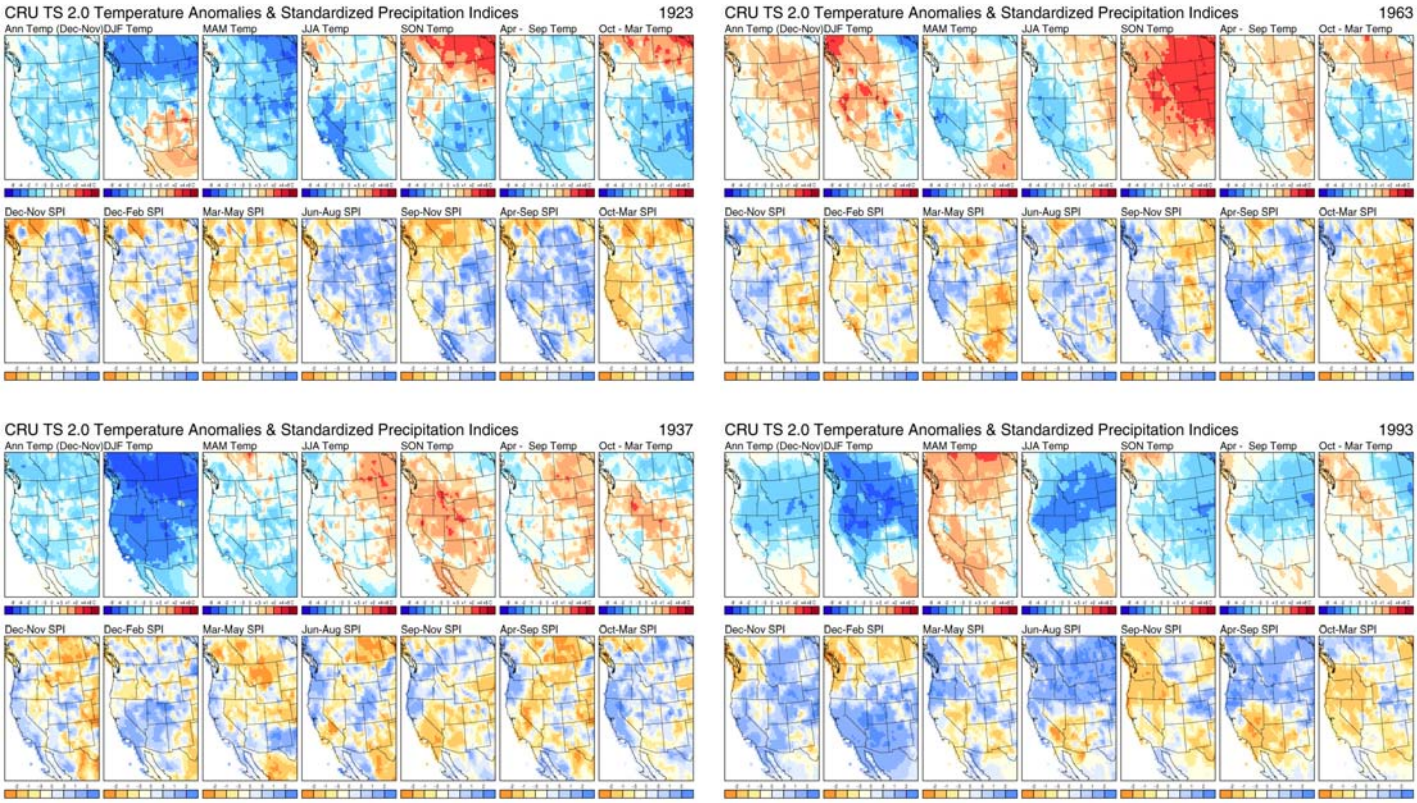


**Figure 16.** Air temperature anomalies and standardized Precipitation Indices for selected high (upper four map sets) and low (lower four map sets) fire years in the 20th century. Refer to Figure 8 for comparison of fire area burned for the selected years.

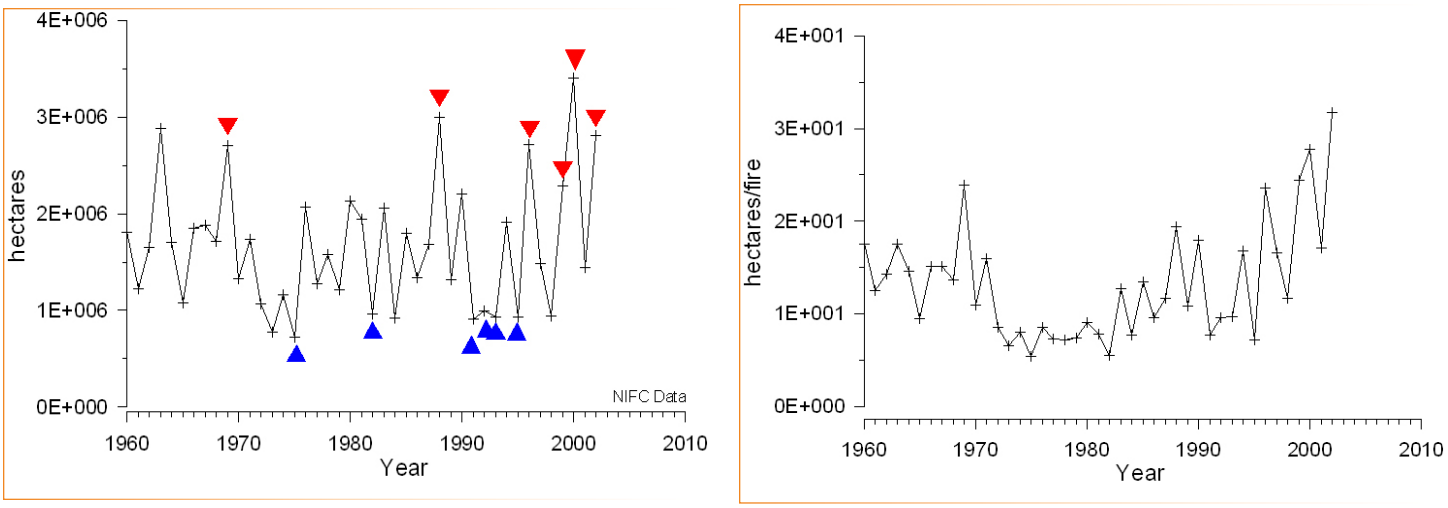


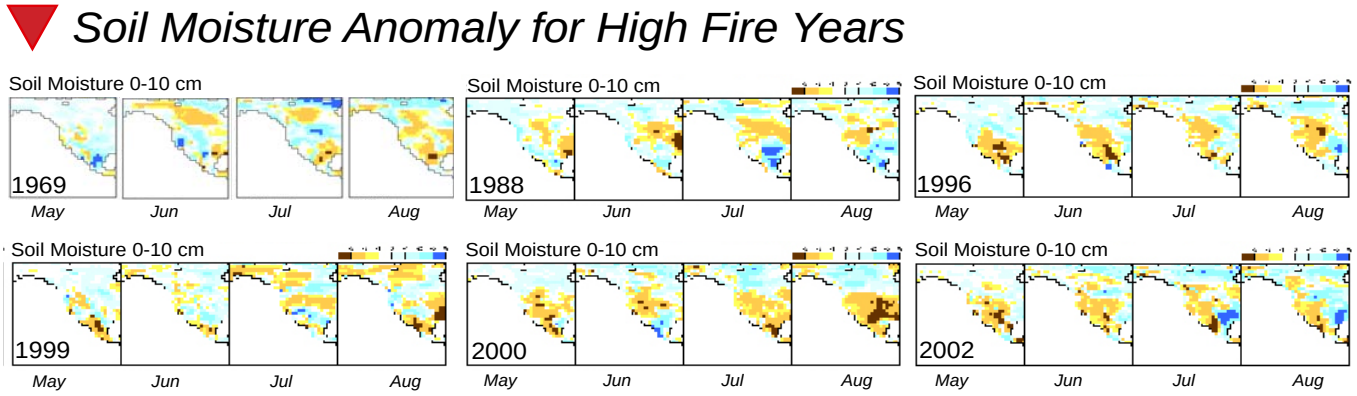


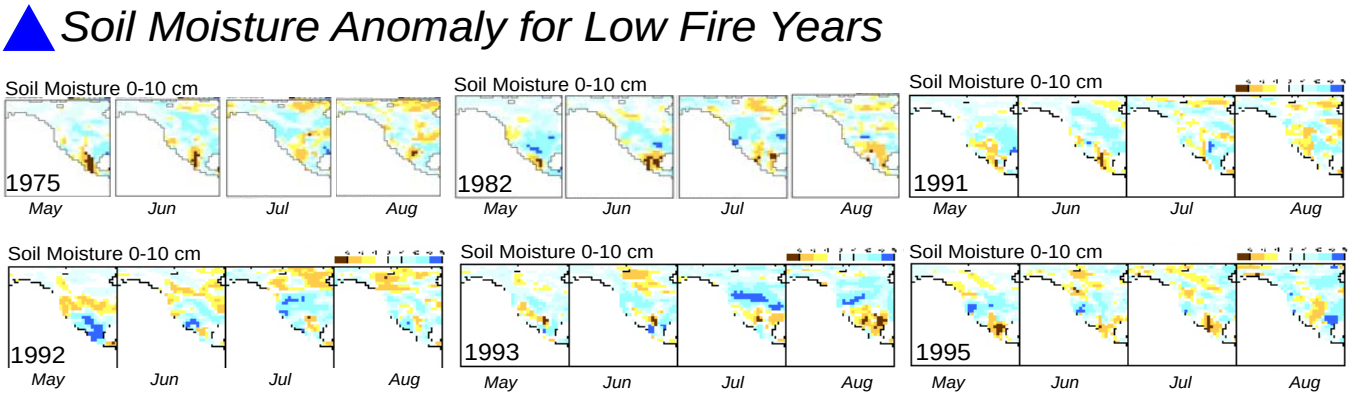


**Figure 17**. Hectares burned (upper graphs) and hectares burned per fire (lower graphs) in the continental US for the period 1960-2002 compared with soil moisture anomaly graphs for selected high (red triangle) and low (blue triangle) fire years. Fire data from NIFC and soil moisture data from the NCEP reanalysis.

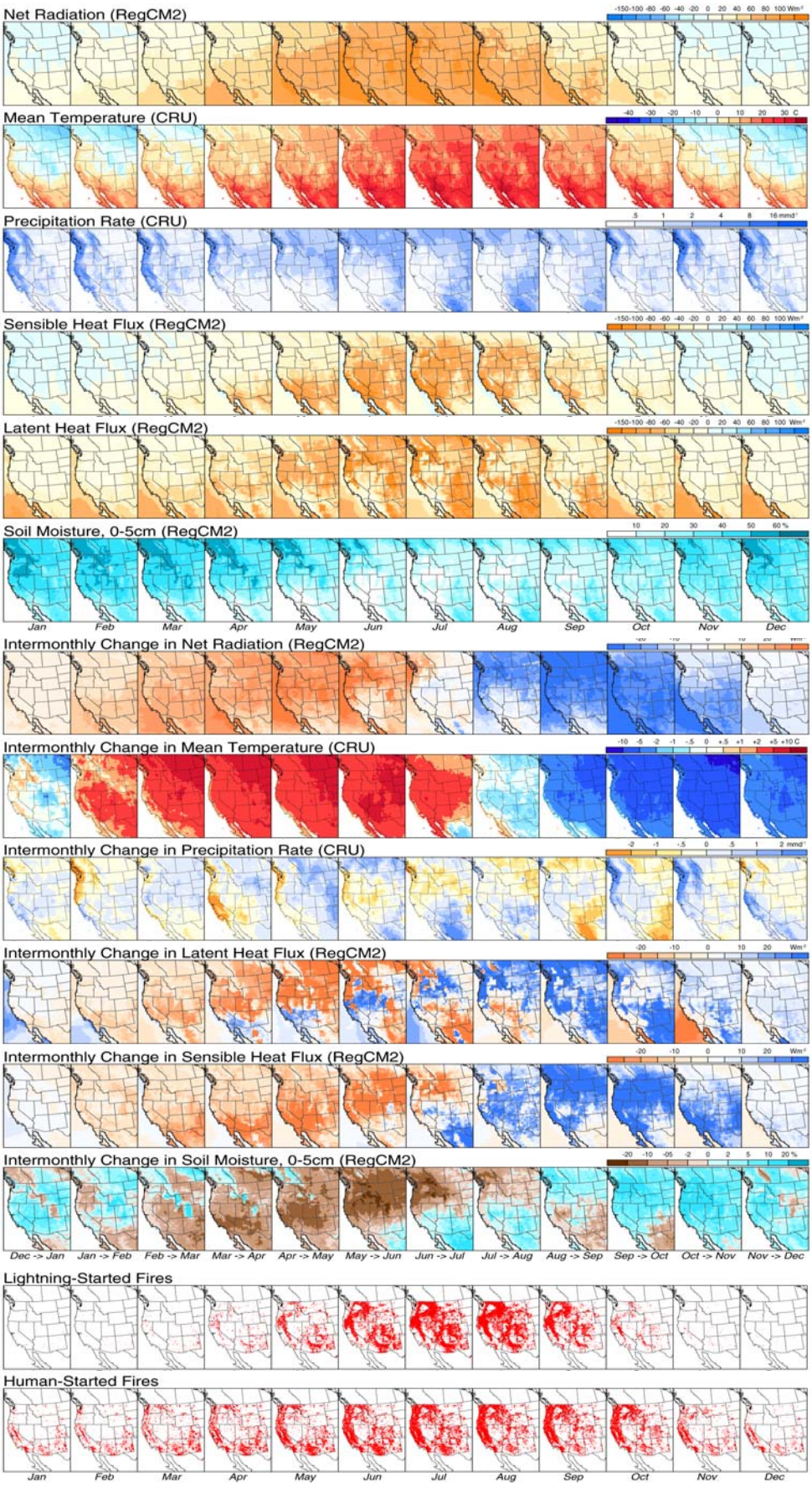


**Figure 18.** The seasonal cycle and intermonthly change in climate and surface variables compared with the seasonal cycle of wildfire occurrence for lightning and human ignition sources. Intermonthly changes are the values of the long-term mean for the current month, minus those for the previous month.

the intermonthly changes in precipitation that are more complicated than those of temperature.

The equatorward advance of the westerlies is quite evident in the month-to-month increases in precipitation along the west coast from September through December, while the subsequent retreat from January through July is more gradual. In contrast, the southwestern monsoon builds from May into August, but then diminishes rapidly in September and October. The intermonthly changes in precipitation throughout the year exhibit some form of opposition between the Pacific Northwest and Southwest, a pattern that can be amplified or damped by interannual climate variations, like those associated with ENSO.

Soil moisture is generally high throughout the region in winter, and in the southeastern part of the region in summer. The relative importance of the supply and demand components of soil moisture can be inferred from the intermonthly changes. In general, the intermonthly change patterns of soil moisture are of large spatial scale, resembling the scale (but not necessarily the pattern) of the intermonthly changes in temperature more than those of precipitation; this suggests a stronger effect on soil moisture of net radiation (to which temperature is related) than of precipitation. Superimposed on the broadscale patterns of intermonthly changes in soil moisture are smaller regions with changes opposite in sign to the broad-scale changes. This scale of features is particularly evident in winter and spring; whereas in winter, below-freezing temperatures in upland areas result in the storage of moisture in snowpack and decreasing soil moisture (as is evident in the December to January intermonthly change), in spring this stored moisture replenishes soil moisture as can be seen in the February-to-March intermonthly change.

### *Soil moisture and fire incidence*

The general patterns of soil moisture variations and their intermonthly changes throughout the year (Fig. 18, page 12) provide an explanation for the distribution of human-started fires relative to lightning-started ones, and for the temporal progression of higher levels of fire incidence from ecoregion to ecoregion (Figs. 10, 12). Human-started fires, which occur at low but still substantial levels throughout the cool season (October to April), are generally confined to the regions of lowest soil moisture during this interval. Increases in human-started fires from February through April across the region (and in particular in southern California, Arizona, New Mexico and southern Colorado) correspond to areas of generally decreasing soil moisture over this interval.

In some areas, such as New Mexico and Colorado, precipitation increases from March through May, while soil moisture continues to decrease, reflecting the growing evaporative demand during spring. The general progression of the region of highest incidence of both lightning- and human-started fires from the SW composite ecoregion to the PNW & NRM ecoregion can be seen to track the area in which average soil moisture levels fall continuously over a two-to-three month period. A continuation of a high incidence of lightning-started fires in the SW in July and August despite increasing soil moisture can be explained by the frequent occurrence of monsoon-generated thunderstorms during those months; human-started fires abruptly decrease in frequency in July and August in that region. The end of the lighting-started fire season and the decrease in the rate of human-started fires in October accompanies the general increase in soil moisture across the region in autumn, as winter precipitation commences and evaporative demand falls.

## *Daily fire occurrence*

The occurrence of daily fire outbreaks depends on both prevailing antecedent climatic and surface conditions, which determine the propensity for burning, and lightning for a source of ignition. Fire spread and ultimate fire size also depend on antecedent conditions and meteorological conditions.

Various measures of convection are in use to indicate potential for lightning. These include the lifted index (LI), which accounts for air parcel lifting and low level moisture; convective available potential energy (CAPE), which is a measure of buoyant lifting of air parcels; and the 700-500 hPa temperature lapse rate ($LR_{700\text{-}500}$), which is a measure of the tendency for vertical motion due to temperature differences in the mid-troposphere. The widely used Haines Index (Haines, 1988) is also a measure of convective lifting that attempts to combine the effects of atmospheric temperature and moisture levels to assess wildfire severity. There are, however, serious questions regarding both the theoretical basis and practical application of the index (e.g., Jenkins, 2002, 2004). Here we rely on the $LR_{700\text{-}500}$ as a measure of convective potential. The index is easily computed from our RegCM data and, in contrast to other indices, is applicable over all of the mountainous West.

The correspondence of daily firestarts with $LR_{700\text{-}500}$ is well illustrated with Hovmöller diagrams which display considerable interannual variability in both fire incidence and lapse rate among the 11 years of data (Fig. 19). Within any year, the overall patterns of firestarts and high and low $LR_{700\text{-}500}$ values are contemporaneous and there is strong association between east-west fire outbreaks, indicated by coherent horizontal streaks in the fire data, and the occurrence of similar streaks of strong $LR_{700\text{-}500}$ values. These patterns, which will be discussed fully below, reflect reoccurring patterns of atmospheric circulation that are the principle sources of convective activity over the region.

The Hovmöller diagrams for firestarts with $LR_{700\text{-}500}$ can be combined with diagrams for precipitation, soil moisture and 2-meter air temperature to diagnose the association of fire starts with contemporaneous and antecedent atmospheric and surface conditions (Fig. 20) for two different fire seasons. The 1986 fire season began earlier than 1996 in mid- to late-May during a period of warm temperatures, reduced precipitation, low soil moisture, and active convection, particularly in the west. Several substantial fire outbreaks occurred during the summer and the fire season extended later into the fall than the 1996 season. Both these outbreaks and the length of the fire season are strongly associated with convective activity, moisture conditions, and temperature.

The 1996 fire season was very active (Fig. 19) with a high number of fires in the eastern half of the region (Fig. 20, 21). Here again, the pattern fire outbreaks corresponds to the climate and surface variables, with a key difference relative to 1986 being extensive dry soil moisture over the higher

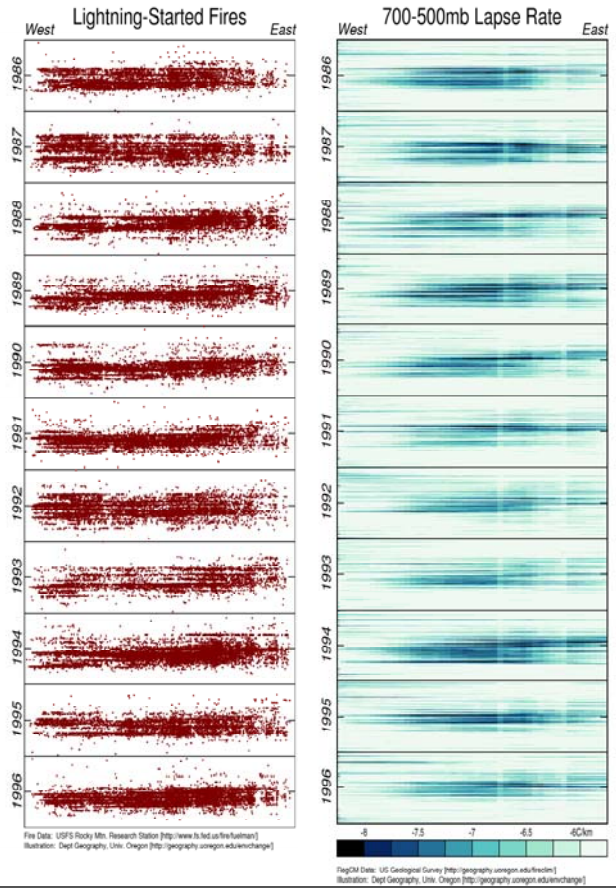


**Figure 19**. Hovmöller diagrams for the 11-year record of daily firestarts and $LR_{700\text{-}500}$ as computed by the RegCM.

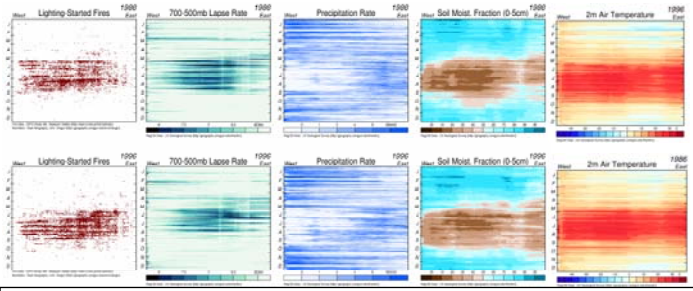


**Figure 20.** Hovmöller diagrams for 1986 (top) and 1996 (bottom) daily firestart data, $LR_{700\text{-}500}$ precipitation rate, soil moisture level, and 2-meter air temperature as computed by the RegCM.

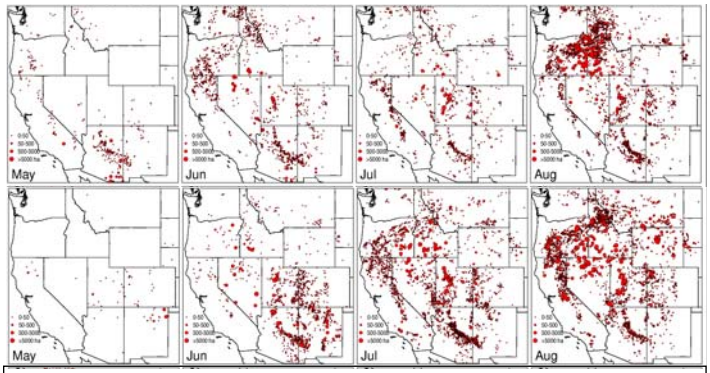


**Figure 21.** May-August spatial patterns of 1986 (top) and 1996 (bottom) daily firestarts

elevations of the Rockies (Fig. 21).

### *Diagnosis of the August, 1996, fire outbreak*

The fire outbreak of August, 1996 provides a good example for diagnosing the temporal and spatial patterns of fire outbreak and atmospheric conditions. We note that this pattern recurs in most fire seasons and is a key mechanism for wildfire in the Sierra Nevada, south Cascades, and Northern Rockies.

Between 7 and 11 August 1996 a weak upper-level trough developed in the Gulf of Alaska and migrated eastward and, at the same time, the subtropical ridge axis along the west coast strengthened and moved inland over the Great Basin. (Fig 22, top row). At the surface the thermal low, also centered over the Great Basin (Fig. 22, row 2), strengthened, so that by 11 August a combination of atmospheric conditions existed that favored the outbreak of fire across the region. These conditions included large-scale rising motions [negative (blue) vertical velocity (omega) values, Fig. 22, row 4], and onshore flow of moisture in the middle and lower atmosphere, which in turn favored development of relatively steep environmental lapse rates (Fig. 22 row 3) and abundant dry and wet convection.

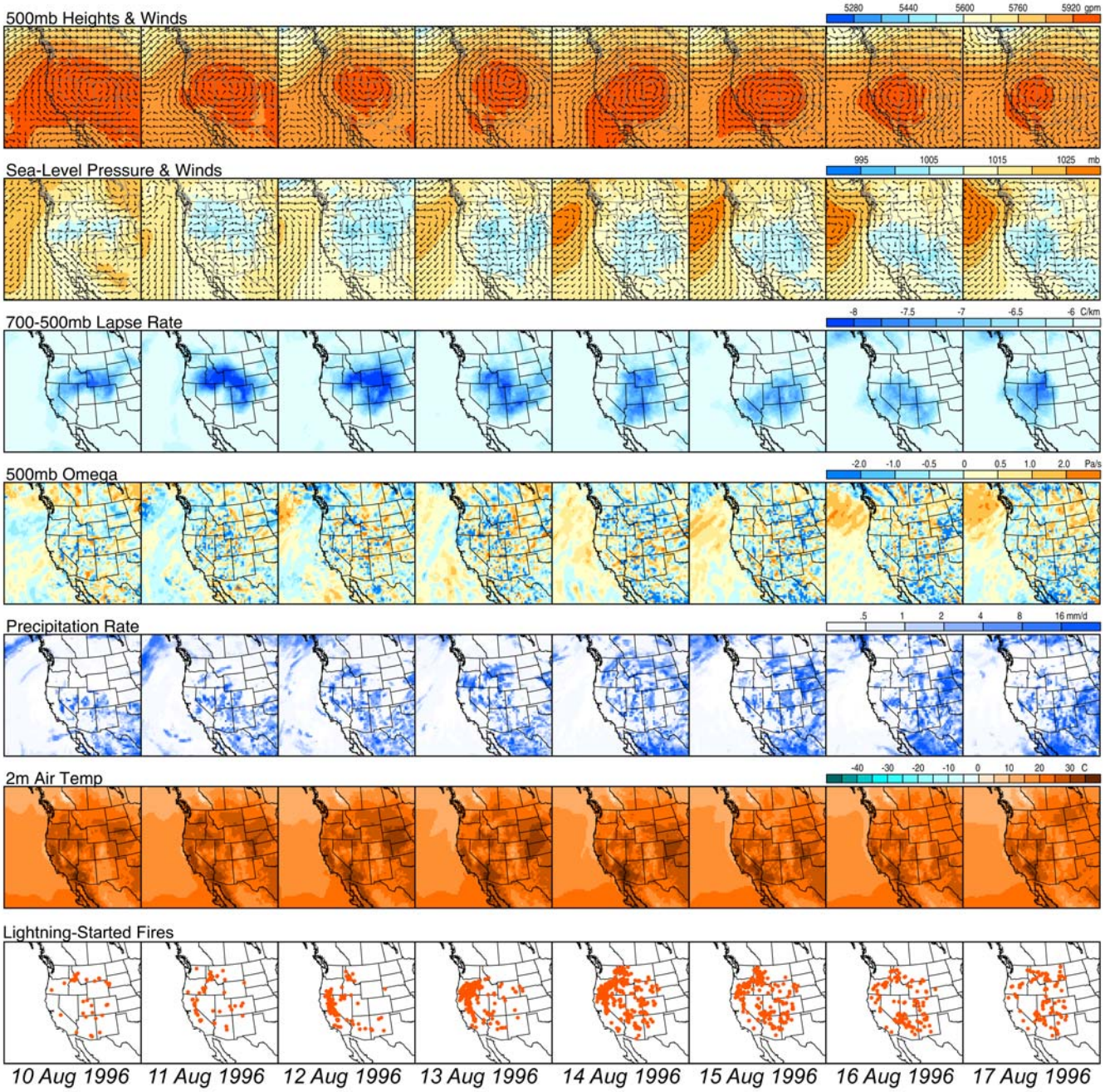


**Figure 22**. Daily patterns of atmospheric circulation, surface climate and fire starts for the period 10-17 August, 1996.

On 12 August, the surface and upper-level circulation produced southwesterly flow into the interior which induced vigorous convective storms. This pattern draws marine air onshore at lower elevations, but is associated with very high fire danger at higher elevations in the Sierra Nevada and Siskiyou mountains. From 13 to 15 August, the subtropical

ridge and thermal low continued to strengthen, resulting in more westerly flow across the northwest into the northern Rocky Mountains. The daily average RegCM fields clearly show the development of this pattern, along with intensification and migration of associated convective indices (700-500 mb lapse rates, and lifted index, not shown). Although there often can be lags between the actual time of a fire start and when the fire is spotted, the temporal and spatial convective precipitation patterns associated with fire starts are well captured by the series of daily convective precipitation patterns from the RegCM.

After 15 August, the subtropical ridge and thermal low weakened and moved southwestward, while the upper-level trough also weakened, ending the convection across the northern half of the region, but reinvigorating the flow of subtropical moisture into the southwest, and increasing convection there.

## *Diagnosis of specific fires*

We designed the atmospheric modeling in this project to enable fire-atmosphere analyses ranging from hourly to decadal in timescales. Here we analyze 1-hour and 6-hour output produced by the RegCM to diagnose the very large Biscuit fire that occurred in southwest Oregon in 2002 and the Yellowstone fires of 1988.

### *The 2002 Biscuit Complex Fire, Oregon*

The Biscuit Complex Fire was comprised of four fires (Biscuit, Sour Biscuit, Florence, and West Florence) that burned together. Accumulated precipitation in southwest Oregon and northern California was far below normal in June, and remained low throughout the summer (Fig. 24). With the exception of a few months, the area received far below normal precipitation since the spring of 2001 as a result of anomalous persistent high pressure over the western US that diverted and blocked precipitation-barring Pacific storms (Fig. 24, lower right). A similar moisture deficit must have existed in small fuels, but, more importantly, moisture deficit in large (1000 hr) fuels made the region particularly vulnerable to large, hot fires.

**Figure 23.** MODIS image of smoke plumes from the Biscuit Fire (lower left plume) and the Tiller Complex Fire (central plume) on 7/31/02 at 19.25 UTC. Image from NOAA MODIS Rapid Response System.

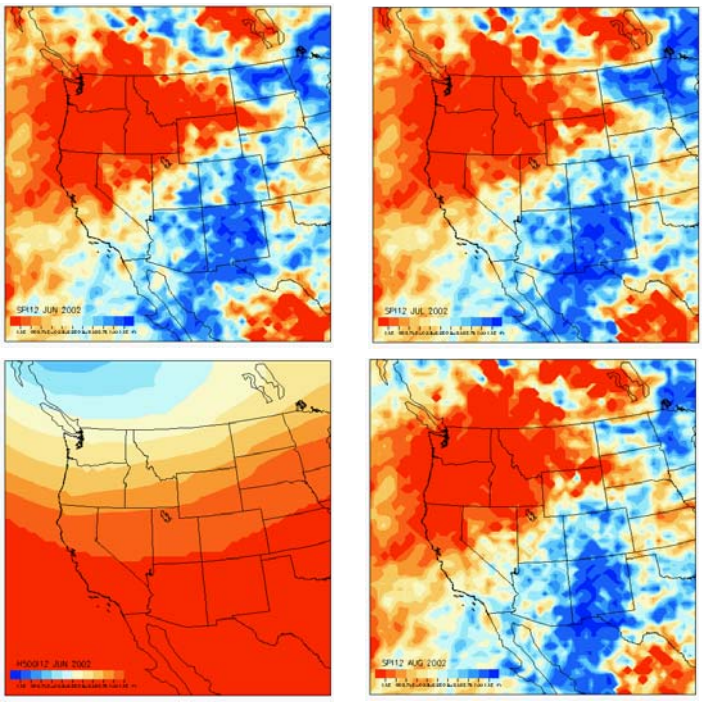

**Figure 24**. Clockwise from the upper left: the 12-month standardized precipitation index for June, July, and August, 2002 and June, 2002 12-month index for 500 hPa heights. RegCM data.

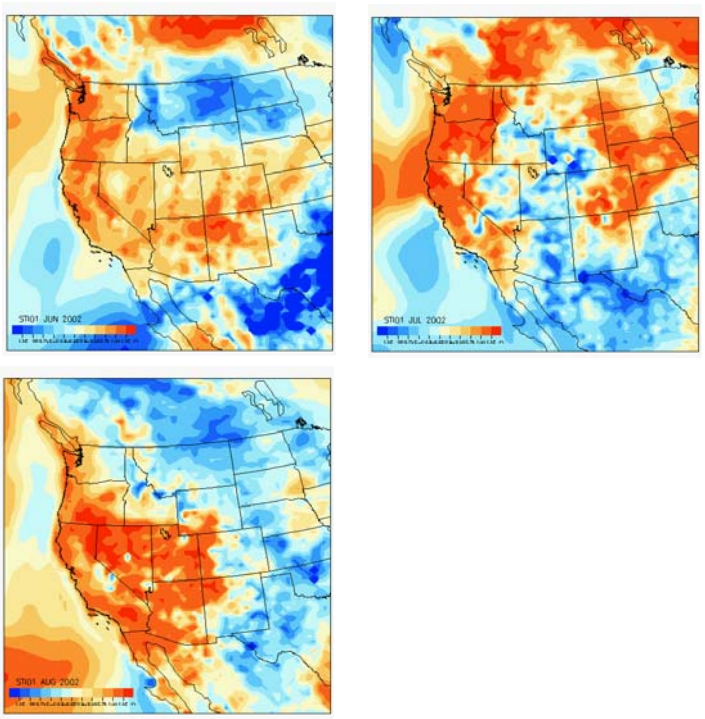

**Figure 25.** Clockwise from the upper left: the 1-month standardized temperature index for June, July, and August, 2002. RegCM data.

In general, the summer of 2002 was very warm over the West. Widespread record high temperatures were set during July, and both July and August temperatures were well above normal over northern California and southwest Oregon (Fig. 25). The July average temperature in Medford, Oregon was 24.8 °C, 0.1 degree less than the record

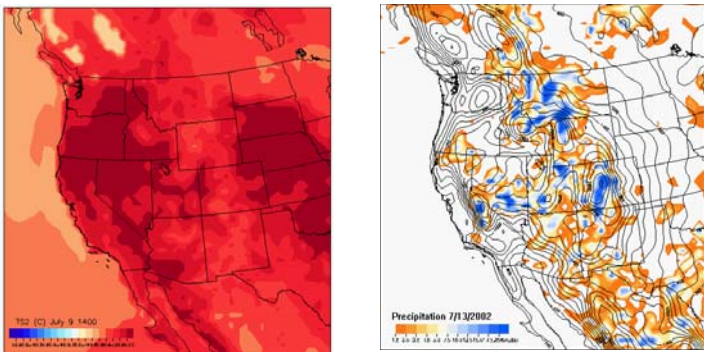


**Figure 26**. RegCM simulated maximum temperature for 1400h, July 9th (left), precipitation for July 13th (right).

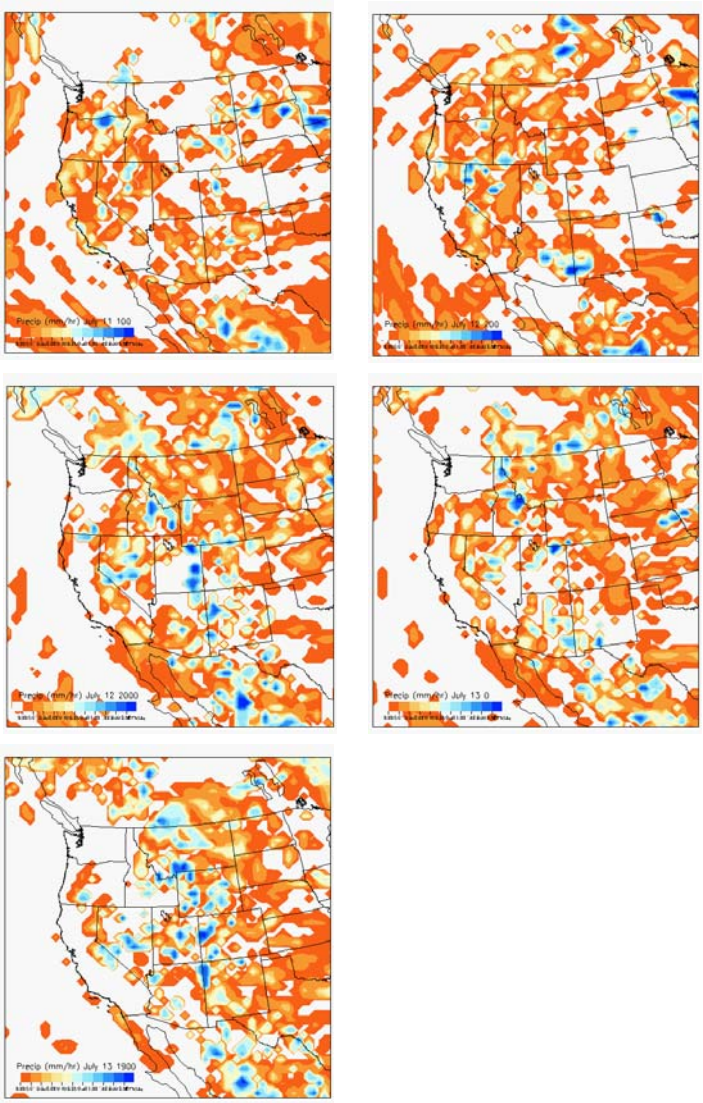

**Figure 27.** Selected hourly (local time) precipitation (convection) as simulated by the RegCM. upper left: July 11, 0100h, upper right: July 12, 0200h, middle left July 12, 2000h, middle right July 13, 0000h, bottom right July 13, 1900h local. The plotting bounds for the precipitation field have been enhanced to emphasize simulated convective activity; precipitation amounts associated with the orange colors range from fractions of mm to around 1 mm.

for the month. High-temperature records were set on July 9th (40 °C) (Fig. 26) and 10th (41°C), preceding the start of the fire. The only measurable precipitation occurred on the 13th and 14th (2.0 mm) (Fig. 26). Continuation of these dry and hot conditions supported severe fire conditions and spread of the fires.

During the week preceding the start of the fire a circulation pattern developed that was very similar to that discussed previously with regard to the August, 1996 daily firestarts. A thermal low developed in the central valley of California and progressed northward bringing hot temperatures and low pressure at the surface. As a combined result of the upper level and surface pressure patterns strong, hot, and dry easterly surface winds that originated east of the Cascades.

This pattern of easterly winds is associated with extreme fire danger in western Oregon. On July 10th, a trough formed aloft off the coast of the Oregon and California coast, resulting in moist, southwesterly wind flow over southwestern Oregon. The advection of moisture led to atmospheric instability (strong divergence in the lower troposphere), strong convection over southwest Oregon and northward along the Cascades (Fig. 27), and the ignition of many fires. In addition to the Biscuit (Florence) fire, the Umpqua National Forest office reported 115 lightning-caused fires were set from late July 12 through July 13. One fire complex (Tiller, Fig. 23) subsequently spread to over 12,140 ha. Once set, hot temperatures and periods of easterly winds during the remainder of July and August favored the spread of the Biscuit fire which ultimately burned 202,350 ha.

### *The 1988 Yellowstone fires*

We illustrate the use of the RegCM output to diagnose the Yellowstone fires by comparing the 1988 fire season with the 1986 fire season. The 1988 fire season was severe

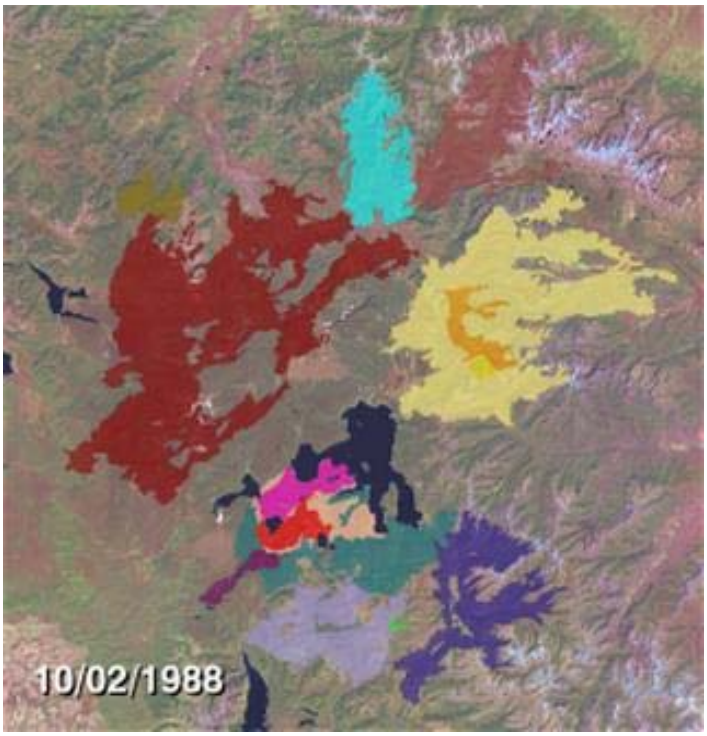


**Figure 28**. False color landsat image of fire area extent at the end of the 1988 fire season in Yellowstone National Park. Colors indicate various fires. Yellowstone Lake is dark blue in the center of the image. Source: NASA/Goddard Space Flight Center Scientific Visualization Studio. Animations of fire spread available at http://svs.gsfc.nasa.gov/search/Keyword/YellowstoneNationalPark.html

in Yellowstone Park: eight lightning-started wildfires ultimately burned ~1 million hectares, about 45% of the park area (Fig. 28 29). In contrast, few relatively small fires occurred in the park 1986.

May of 1988 was unseasonably cool in the Yellowstone

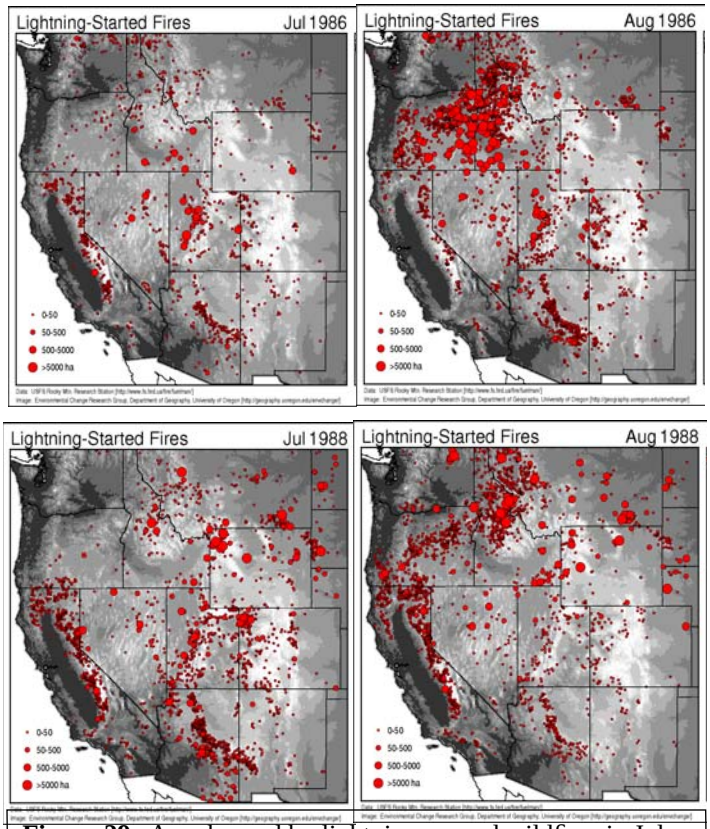


**Figure 29**. Area burned by lightning-caused wildfires in July and August of 1986 (top) and 1988 (bottom).

region (Fig. 30); however, cool conditions were immediately followed by abnormally warm temperatures in June, July, and August. In addition, As a result of a persistent ridge over the Northwest (Fig. 31, lower left) the region

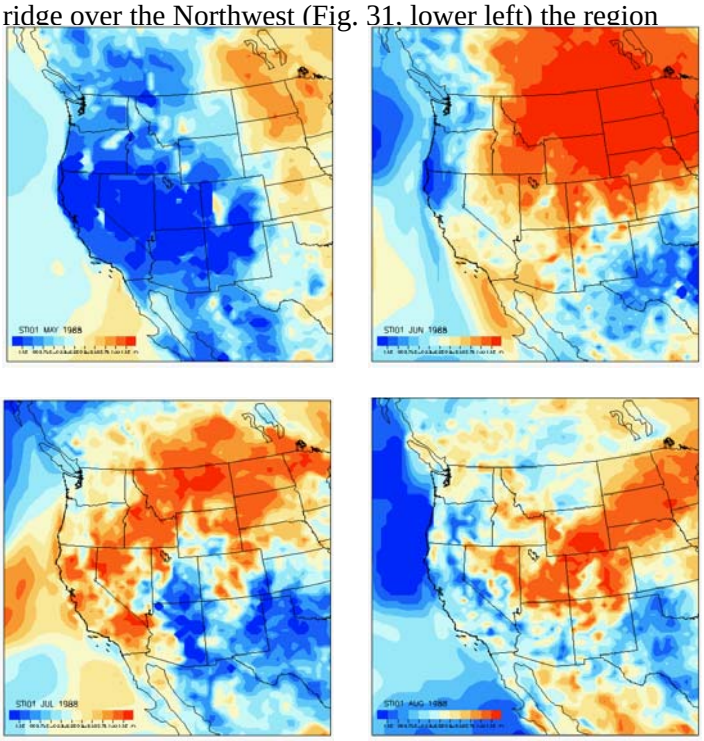


**Figure 30**. Clockwise from upper left: Temperature departure from normal (STI) for May, June, July, and August, 1988. Data from RegCM.

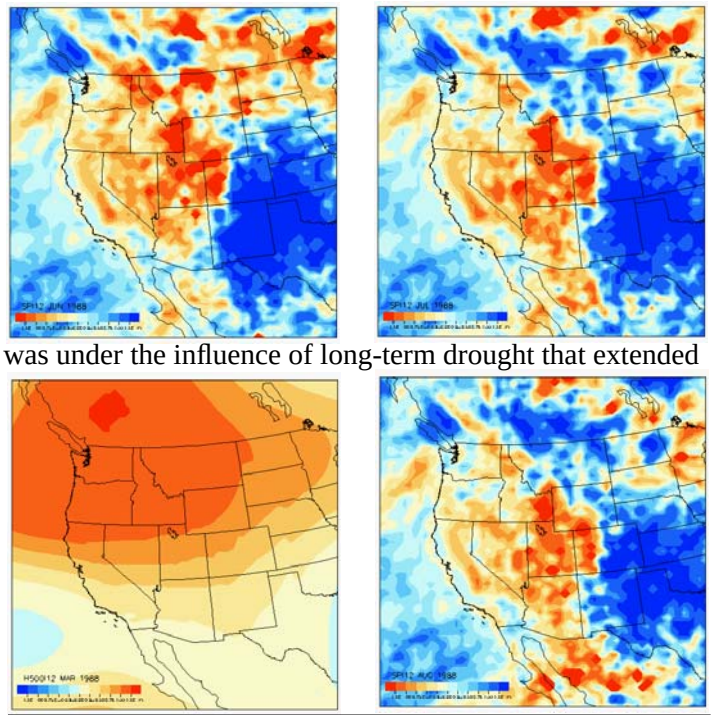

was under the influence of long-term drought that extended

**Figure 31**. Clockwise from upper left: 12-month precipitation departure from normal (SPI) for June, July, and August, and 12-month departure from normal 500 hPa heights for 1988. Data from RegCM.

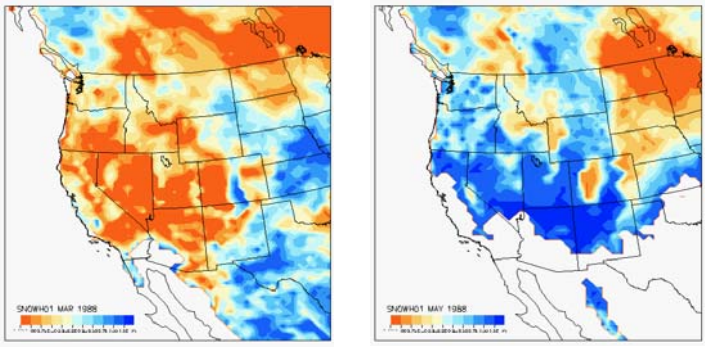


**Figure 32.** Snow depth departure from normal for March (left) and June (right), 1988. Data from RegCM.

back to the previous 12 months and continued throughout the 1988 fire season (Fig. 31). Over the West, March, 1988, snowpack was generally below normal with large departures in the Yellowstone region (Fig. 32). Wet and cold conditions in May ameliorated the low snowpack somewhat, but low snowdepths in the Yellowstone persisted.

Conditions favoring the 1988 fire season began with early melting of the winter snowpack as a result of unseasonably warm temperatures that began in late May (Fig. 33). Throughout summer, vegetation temperatures remained very high, relative humidity was low, precipitation was minimal and soil moisture levels were very dry, setting up favorable conditions in dead and live fuels for wildfire. As indicated by precipitation and the variability of sea level pressure (SLP, Rorig and Ferguson, 1999, 2002) and wind in 1988 a number of convection-producing fronts (high to

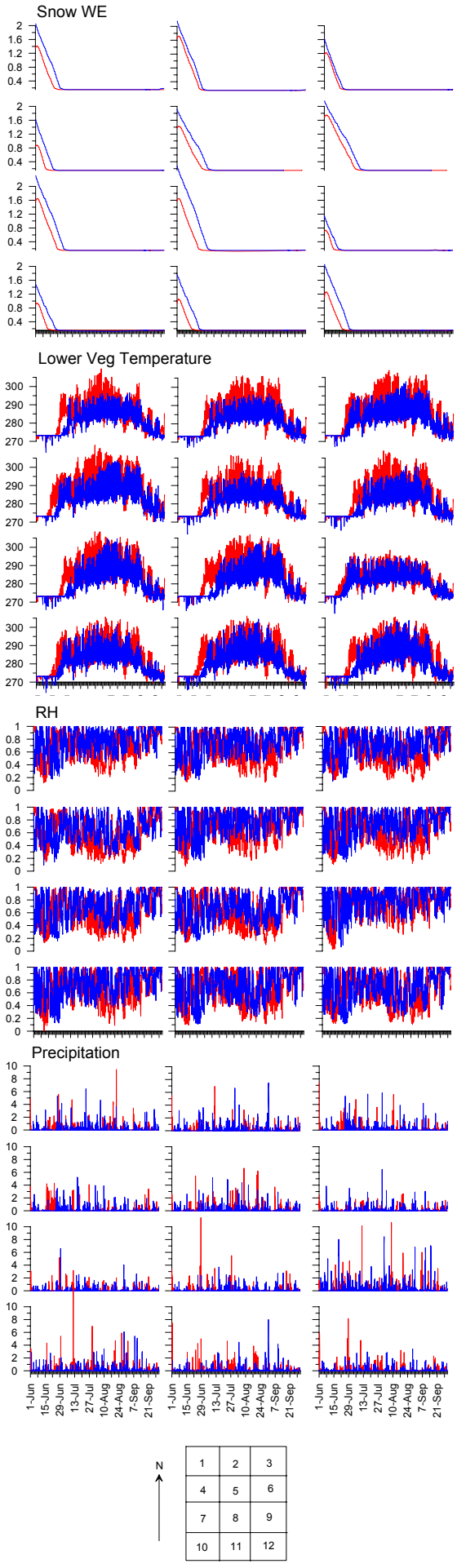


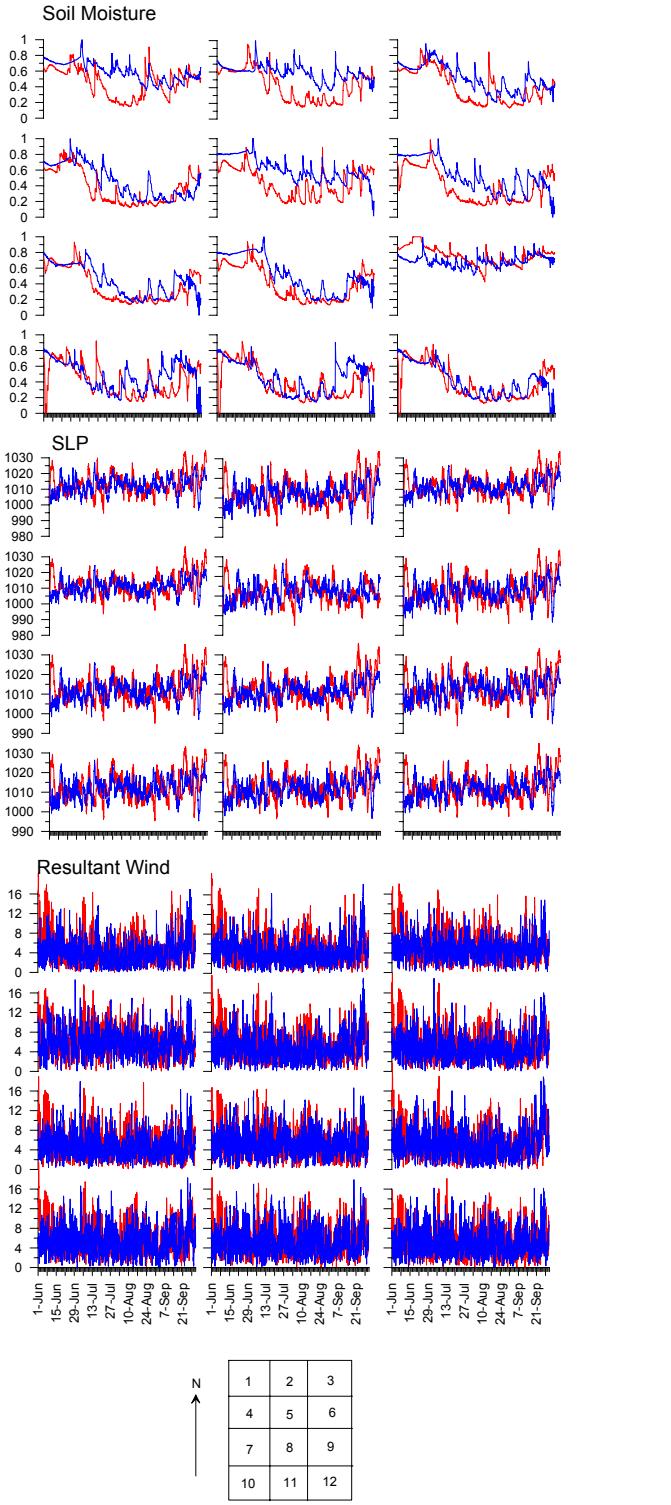


**Figure 33.** June through September, 1988 (red) and 1986 (blue) time series of hourly meteorological and surface variables for the Yellowstone National Park area. For each variable, data are displayed for each of the 9 RegCM grid cells that surround the park area. The temperature plot is for the temperature of the lower vegetation as simulated by the land surface package in the RegCM. As indicated by the map key, the grid cells are arranged in rows from north to south.

low SLP) passed over the area in July and August. Once the fires were set, our simulations indicate that persistence of warm temperatures, low relative humidity, very low soil moisture levels, and high winds over much of the area supported expansion and spread of the fires. The combined results of our simulation are consistent with other analyeses of the 1988 fires (Christinsen et al., 1989; Romme and Dispain, 1989; Rothermel, 1991).

As we have demonstrated earlier, an advantage of the RegCM is the ability to simulate and output the complete surface energy balance. The use of the surface energy balance to diagnose fire conditions is a relatively new method that we believe is promising. To demonstrate this approach, we have plotted the 6-hour time series of sensible heat and soil moisture for the summer of 1988 (Fig. 34). Net radiation absorbed at the surface is divided between latent heat flux (evaporation) and sensible heat (the ratio of latent to sensible heat flux is called the Bowen ratio). Thus, when soil and fuel moisture levels are high, sensible heat flux is generally low because more absorbed radiation is being expended by evaporation and evapotranspiration in the form of latent heat. The effect is most evident following precipitation and slight replenishing of soil moisture. During the prolonged period of low soil and fuel moisture during July and August, however, sensible heating is very high. The addition of sensible heat to the energy balance of enhances fire conditions (e.g., Snyder et al., 2003) and, in the forest canopy, supports the development of crown fires (e.g., Clark et al., 2005)

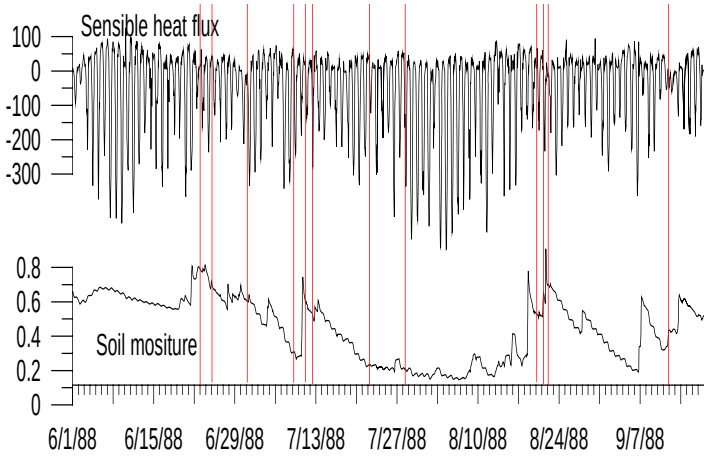


**Figure 34**. June- September, 1988, 6-hour sensible heat flux and soil moisture levels averaged over the 9 RegCM grid cells. Dates of major fire starts are indicated by the vertical lines. Negative values of sensible heat indicate the flux is away (upward) from the surface.

***Summary***

Our diagnosis and analysis of historical fire and climate data presented here and in the atlas demonstrate and identify mechanisms that link wildfire and climate in the western US over a wide range of temporal and spatial scales. Our methodologies clearly have further applications. An obvious application of this work is in the area of monitoring atmospheric and surface conditions over monthly and longer time periods as a means of evaluating regional wildfire potential for a coming fire season. Toward this goal, we are keeping up-to-date with our regional climate model simulations as the NCEP reanalysis is made available by NOAA and we are current with our analyses of present and antecedent conditions. We are also exploring spatial/temporal statistical methods that we will use to quantify key associations. We thus hope to augment season-ahead fire forecasting efforts.

Another application of our research will be in the area of assessing the sensitivity of wildland fire to climate conditions of the past and future. In preliminary work, we have already demonstrated that our analyses are useful for linking the geologic record of wildfire (e.g., charcoal records) to past climates simulated by climate models. Because we conduct many such climate model simulations we are ideally positioned to focus on past and future wildfire and climate research.

A crucial component of past and future wildfire-climate research is incorporating static and dynamic vegetation models to account for vegetation changes induced by climate and increased atmospheric trace gas concentrations. As we demonstrate in the following two sections, we have begun these modeling activities on various scales.

## *Modeling the effects of fire frequency and severity on forests in the northwestern United States (EPA component)*

Across the Pacific Northwest, forests are subject to a wide diversity of fire regimes (Agee, 1993). It follows that the region is well-suited for investigation of the effect of contrasting fire regimes on forest dynamics. We use an enhanced version of the FORCLIM forest model (Bugmann, 1996) to investigate how fire severity and frequency affect forest composition and structure in the Pacific Northwest over long time periods. The model operates on time scales from years to centuries tracks the species and size of tree stems, and includes the effects of climate on trees (Bugmann and Solomon, 2000). With the added capability of simulating fire frequency and severity FORCLIM becomes particularly useful in the western US.

### *Study region*

To evaluate the model and simulated fire effects we chose a series of eight ecoregions along a broad climatic gradient in western Oregon from the Pacific Coast to the interior (Fig. 35). Fires are very infrequent in wet, coastal forests. Forests and rangelands of interior Oregon experience dry summers and have much higher fire frequencies resembling those of much of the western US.

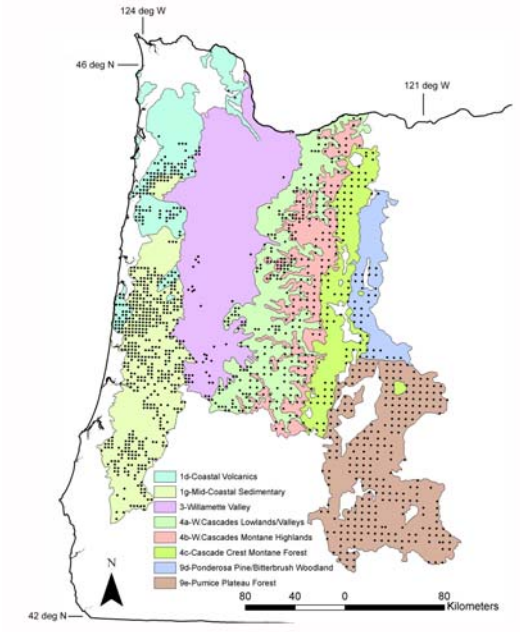


**Figure 35**. Map of western Oregon showing the eight forested ecoregions studied for fire regime effects.

### *Empirical data*

In order to assess the existing vegetation of western Oregon a set of data on 2323 forest stands in the region (Fig. 35) were assembled from USDA and USDI databases (Busing, 2004). We calculated basal area for dominant species and for all species combined. Stand age, or time since the last stand-replacing disturbance, was estimated as the maximum age of a cored tree at each plot site. Climate data were assigned to each plot site using the geographic coordinates of the plot and the interpolated climate data sets described in Lugo et al. (2000).

### *The model*

Assessments of simulated forest composition along climatic gradients have demonstrated the wide applicability of advanced versions of FORCLIM in temperate forest regions (Bugmann and Solomon, 2000). The model generates tree species composition along climatic gradients that tends to follow patterns of potential natural vegetation (sensu Kuchler, 1964) in several regions, including the Pacific Northwest (Franklin and Dyrness 1988). It also simulates forest response to changing regimes of climate and disturbance (Busing and Solomon, 2004, 2005).

Unique features of FORCLIM 2.9, a version developed for the strongly seasonal climate of the Pacific Northwestern United States, center on the effects of climate on tree performance (Bugmann and Solomon, 2000). A pool of 18 tree species (20 taxa when two subspecies are distinguished) common to northwestern Oregon is used in this study (Bugmann and Solomon, 2000; Busing and Solomon, 2004). Key species parameters affecting vegetation dynamics include a maximum diameter at breast height (DBH), a maximum age, a unique set of resource-growth-response functions, and a set of conditions for ingrowth.

We enhanced the FORCLIM 2.9 model to simulate effects of fire frequency and severity. Species were assigned to one of four fire tolerance classes based on information provided by Minore (1979) and the USDA Fire Effects Database. The least fire tolerant class contained *Abies amabilis, Abies lasiocarpa, Chamaecyparis nootkatensis, Picea engelmannii, Picea sitchensis, Tsuga heterophylla,* and *Tsuga mertensiana*. These species (class 1) were subject to complete stand-wide mortality during a fire event regardless of fire severity. For the three remaining classes of tolerance, fire effects were simulated so that large trees had greater survivorship than small trees (Dale and Hemstrom, 1984). Species in the mildly tolerant category (class 2) (*Abies grandis, Abies procera, Acer macrophyllum, Alnus rubra, Arbutus menziesii, Pinus contorta, Pinus monticola* and *Thuja plicata*) suffered heavy mortality, particularly in severe fires. *Pseudotsuga menziesii* was the sole species in the moderately tolerant category (class 3). It suffered low to intermediate levels of mortality depending on stem size and fire severity. Trees in the highly tolerant category (class 4), containing *Pinus ponderosa* and *Quercus garryana*, were subject to relatively low mortality from fire events.

Fire regimes were typically simulated as a combination of low-severity and high-severity events. Simulated events of low severity had little impact on mortality of larger trees of fire-resistant species. However, trees of fire-intolerant

species and small trees of species with low to moderate fire tolerance were impacted by events of low severity as well as those of high severity. The likelihood of tree mortality among fire-resistant species (classes 2-4) increased with fire severity.

### *Model comparisons with field data*

The ability of FORCLIM 2.9 to generate accurate vegetation patterns across environmental gradients was tested using the forest survey data set. The test involved older forest sites surveyed within selected ecoregions representing much the variation in precipitation, temperature, and natural disturbance in western Oregon forests. Critical input parameters varied among simulations were site monthly mean climate, in certain cases, annual fire disturbance frequency and severity, and simulation length (yr). Species parameters were not varied among simulations.

The tests focused on eight forested ecoregions in western Oregon. Forested ecoregions (Omernik classification; Thorson et al., 2002) centered north of 43° N latitude and having 20 or more field data sites with old trees (>150 yr) were used in the analysis (Fig. 35). In the Willamette Valley (ecoregion 3), where survey data on old stands were scarce, data from stands with trees approaching or exceeding 100 yr in age were collected to supplement the survey data set. For each ecoregion, measured basal area of dominant species, and the entire stand served to quantify composition and stand dimensions. We randomly selected a subset of field plot sites (n=20) within each ecoregion. Prior to the simulations, the selected field sites were demonstrated to represent the larger pool of eligible field sites available in the ecoregions

Initial simulations were based on climate regime and age of the oldest tree (which dictated simulation length) at each randomly selected site. In additional simulations, regimes of fire disturbance were superimposed on the stands. Various regimes of fire, differing in disturbance frequency and severity, characteristic of each ecoregion were simulated. Fire return intervals ranged from 15 to 400 yr (frequency 0.067 to 0.0025 yr-1). Fire regimes ranged from severe events with long return intervals (mean 400 yr) in ecoregions 1d and 4c to those dominated by low severity events with short return intervals (15 yr) in ecoregions 3, 9d and 9e.

### *Forest basal area*

The simulations lacking fire gave total basal area values that exceeded actual values. Simulated mean basal area was higher than the actual mean basal area in each of the eight ecoregions (Fig. 36a and b). When appropriate fire regimes were simulated for each ecoregion, the agreement between simulated and actual mean basal area improved markedly (Fig. 36c). The sharp decline in total basal area in the Willamette Valley (ecoregion 3) was captured only by simulations with fire. Similarly, only the simulations including fire approximated the low total stand basal area in the Pumice Plateau (ecoregion 9e).

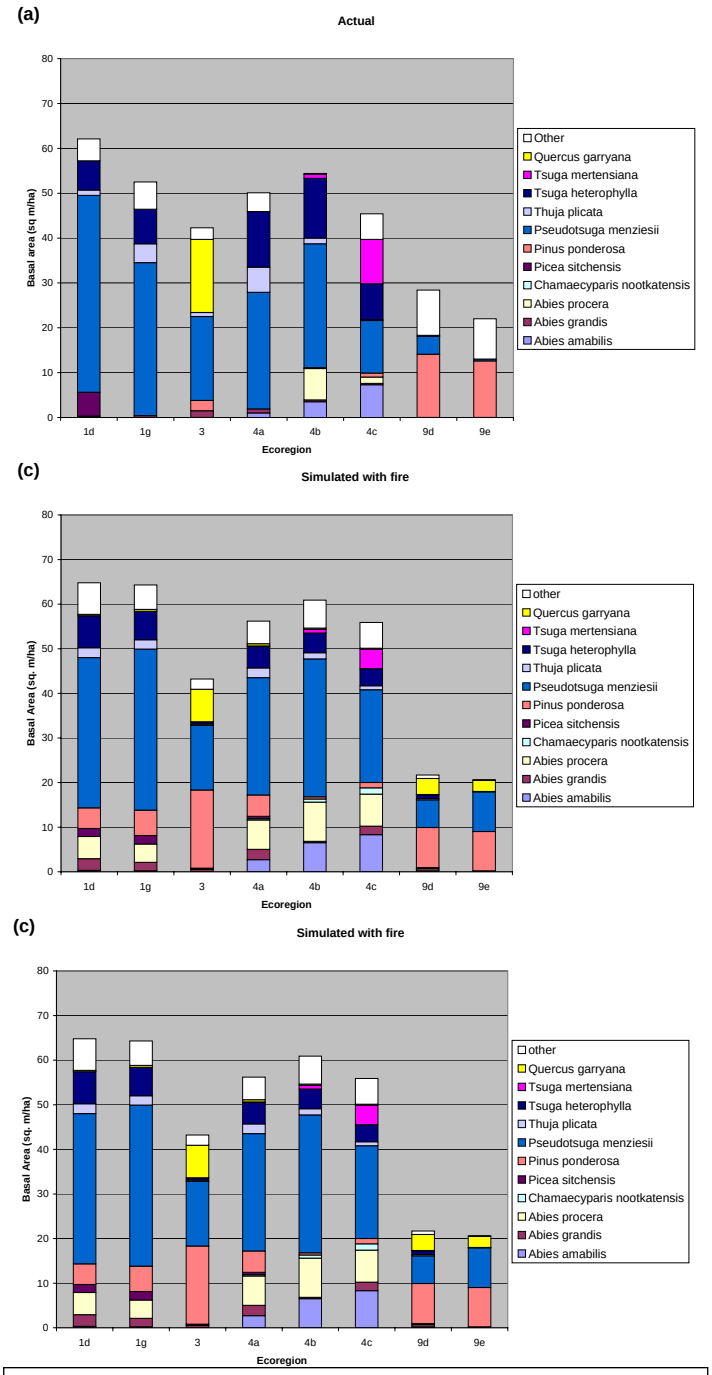


**Figure 36**. Graphical comparisons of forest basal area and composition by ecoregion among a) actual data, b) simulated data without fire, and c) simulated data with fire. Each vertical bar represents an ecoregion (see Fig. 35) from the Pacific coast (left) to interior Oregon (right).

### *Forest composition*

The observed data showed a shift in tree species composition from *Pseudotsuga* dominated forests in coastal and montane regions of western Oregon (ecoregions 1-4) to *Pinus* dominated forests in central Oregon (ecoregions 9d & e) (Fig. 36). An increase in subalpine conifers was evident at high elevations of the Cascade Crest (ecoregion 4c). Simulations without fire gave forests dominated by *Pseudotsuga* in all eight ecoregions studied. It was clearly

overestimated in drier forests with high frequencies of low-severity fires (ecoregions 3, 9d & 9e). Simulations with high fire frequencies reduced the levels of *Pseudotsuga* and increased the relative dominance of very fire-tolerant species such as *Pinus ponderosa* and *Quercus garryana*. With the addition of fire to the simulations the only major discrepancy between actual and simulated composition is the abundance of *Pinus ponderosa* in the simulated forests of the Willamette Valley (ecoregion 3) (Fig. 35). Although *Pinus ponderosa* occurs in the valley it is not currently a dominant species. It may have been more important prior to European harvesting and fire suppression (Johannessen et al. 1971).

Fire effects, simulated by elevating the mortality of trees based on their species and size, alter forest structure and composition. Low frequency fires (return interval >200 yr) have minor effects on composition. When they are severe, they tend to reduce total basal area. In the current study, simulated basal areas were reduced to levels approximating actual basal areas. High frequency fires (return interval <30 yr) have major effects on composition and on total basal area. They can cause substantial reductions in total basal area and shifts in dominance toward highly fire tolerant species.

### *Modeling climate and fire in ecosystems of western North America (USGS-EPA component)*

Simulation of vegetation and ecosystem effects of climate and fire on a large scale was accomplished with the Lund-Potsdam-Jena (LPJ) model (Sitch et al., 2003). This dynamic global vegetation model (DGVM) was run over western North America. The fire routine in the model depends on litter moisture, fuel load and fire season length to estimate the potential fraction of area burned in each simulation cell in a given year (Thonicke et al. 2001). Thonicke et al. validated the fire routine for European fire-climate relationships. Its reliability in western U.S. systems has been questioned (Bachelet et al. 2003) so a suitable implementation of a wildfire routine in LPJ remains a focus of our collaborative work.

As a first attempt at using LPJ as a climate-driven model for fire simulation, we ran the model for the period 1986-1996 using the CRU temperature and precipitation data. The model was initialized and run for approximately 500 years before the 1986-1996 annual fire behavior was simulated. The results capture aspects of the inter-annual variation in annual fractional area burnt for western North America (Fig. 36). For example, in 1988, the year of the large Yellowstone fires, the model correctly simulates higher potential area burned for the Yellowstone region as compared to other years in the record. The model is currently limited, however, in that it assumes an ignition source will occur in every grid cell at some point during the year. Yet lightning, the predominant non-human fire ignition source in the western US, occurs more frequently in certain areas of the region than in others. As a result, there is not a good spatial match between the area burned simulated by LPJ and the observed distribution of fires. The model also appears to overestimate fuel load in parts of the southwest, as indicated by large burned areas simulated in regions where the vegetation tends to be too sparse to carry fires over large areas.

Both the intra- and inter-annual processes modeled in the LPJ fire routine require further examination with regard to simulating fire occurrence in the western U.S. Additional work is also needed to improve the model's simulation of the spatial distribution of both ignition sources and fuel load. Identification and application of the general links between climate and fire in ecosystem models of the United States remains a challenge

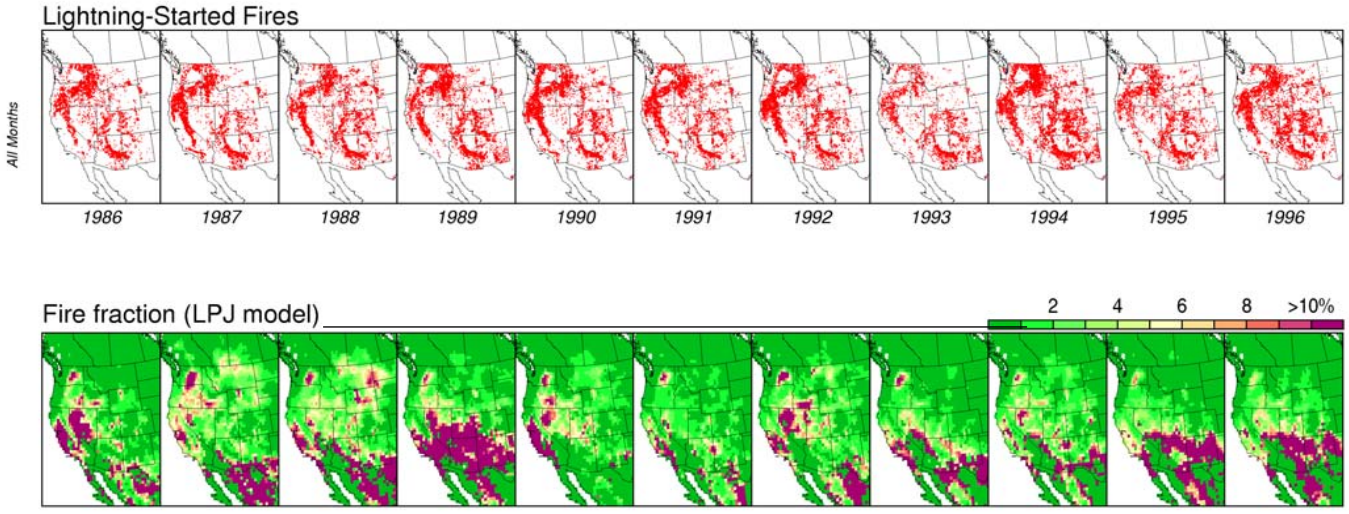


**Figure 37**. Figure 37. Lightning-caused fire starts from 1986 to 1996 (top) and fire fraction simulated with the LPJ model (bottom) for the same set of years.

## *References*


Agee, J.K. 1993. Fire ecology of Pacific Northwest forests. Island Press, Washington, D.C.

Bartlein, P.J., S.W. Hostetler, S.L. Shafer, J.O. Holman, and A.M. Solomon, 2003: The seasonal cycle of wildfire and climate in the western United States, 5th Symposium on Fire and Forest Meteorology, Meteorological Society, paper P3.9.

Batchelet, D., R. P. Neilson, T. Hickler, R. J. Drapek, J. M. Lenihan, M. T. Sykes, B. Smith, S. Sitch, and K. Thonicke, 2003: Simulating past and future dynamics of natural ecosystems in theUnited States. Global Biogeochemical Cycles, 17:1045. doi:10.1029/2001GB001508

Brown, J.K. and C.D. Bevins, 1986: Surface fuel loadings and predicted fire behavior for vegetation types in the Northern Rocky Mountains. USDA For. Serv. Res. Note INT-358, Intermountain For. and Range Expt. Sta., Ogden UT, 9 p.

Brown, T. J., B. L. Hall, C. R. Mohrle, and H. J. Reinbold, 2002: Coarse assessment of federal wildland fire occurrence data. Desert Research Institute, Program for Climate, Ecosystem and Fire Applications, Report CEFA 02-04, 31 pp., http://www.cefa.dri.edu/Publications/fireoccurrencereport.pdf (accessed August 24, 2003).

Bugmann, H.K.M. 1996: A simplified forest model to study species composition along climate gradients. *Ecology* 77: 2055-2074.

Bugmann, H.K.M., and A.M. Solomon, 2000: Explaining forest composition and biomass across multiple biogeographical regions. *Ecol. Appl*. 10:95-114.

Busing, R.T. 2004: A vegetation database for western Oregon. U.S. Geological Survey Open File Report OF 2004-1249.

Busing, R.T., and A.M. Solomon, 2004: A comparison of forest survey data with forest dynamics simulators FORCLIM and ZELIG along climatic gradients in the Pacific Northwest. U.S. Geological Survey Scientific Investigations Report 2004-5078.

Busing, R.T., and A.M. Solomon, 2005: Assessment of a model of forest dynamics under contrasting regimes of climate and disturbance in the Pacific Northwest. U.S. Geological Survey Scientific Investigations Report 2005-5242

Christensen NL, JK Agee, PF Brussard et al. 1989: Interpreting the Yellowstone fires of 1988. *BioScience* 39: 678–85.

Clark, K.L., J. Horn, and N. Skowronski, 2005: Not so barren. *Wildfire Magazine*, May, 1.

Cole, J.E., and E.R. Cook, 1998: The changing relationship between ENSO variability and moisture balance in the continental United States. *Geophysical Research Letters* 25: 4529-4532.

Dale, V. H. and M. Hemstrom. 1984: CLIMACS: A computer model of forest stand development for Western Oregon and Washington. USDA Forest Service Research Paper PNW-327.

Edwards, D.C. and T.B. McKee, 1997: Characteristics of 20th century drought in the United States at multiple time scales. Colorado State University, Department of Atmospheric Sciences Atmospheric Sciences Paper 634, Climatology Report 27, 10 pp.

Hardy, C. C., K. M. Schmidt, J. P. Menakis, and R. N. Sampson, 2001: Spatial data for national fire planning and fuel management. *International Journal of Wildland Fire*, 10**,** 353-372.

Hostetler, S.W., P.J. Bartlein, J.O. Holman, A.M. Solomon, and S.L. Shafer 2003: Using a regional climate model to diagnose climatological and meteorological controls of wildfire in the Western United States, 5th Symposium on Fire and Forest Meteorology, American Meteorological Society, paper P1.3.

Hovmöller, E. 1949: The trough and ridge diagram. *Tellus*, 1:62-66.

Flannigan, M., B. Todd, M. Wotton, B. Stocks, W. Skinner, and D. Martell, 2000: Pacific sea surface temperatures and their relation to area burned in Canada. Preprints, Third Symposium on Fire and Forest Meteorology, American Meteorological Society, Boston, pp. 151-157.

Franklin, J.F., and C.T. Dyrness, 1988: Natural vegetation of Oregon and Washington. Oregon State Univ. Press, Corvallis, OR.

Gershunov, A. and T.P. Barnett, 1998: Interdecadal modulation of ENSO teleconnections. *Bulletin of the American Meteorological Society*, 79: 2715-2725.

Giorgi, F., M. R. Marinucci, and G. T. Bates, 1993: Development of a second-generation regional climate model (RegCM2). Part I: Boundary-layer and radiative transfer processes. *Monthly Weather Review*, 121:2794-2813.

Goens, D.W. and S.A. Ferguson, eds., 2000: Third Symposium on Fire and Forest Meterorology Preprints, American Meterological Society, 165p.

Guttman, N.B., 1998: Comparing the Palmer drought index and the standardized precipitation index. J. *American Water Resources Association*, 34(1):113-121.

Guttman, N.B., 1999: Accepting the standardized precipitation index: a calculation algorithm. *J. American Water Resources Association*, 35(2):331-322.

Haines DA, 1988: A lower atmospheric severity index for wildfires. *National Weather Digest*, 13:23–27.

Harmon, M.E. and J. Sexton, 1995: Water balance in conifer logs in early stages of decomposition. *Plant and Soil*, 172:141-152.

Hayes, M.J., M.D. Svoboda, D.A. Wilhite, and O.V. Vanyarkho, 1999: Monitoring the 1996 drought using the standardized precipitation index. *Bulletin of the American Meteorological Society*, 80:429- 438.

Jenkins MA, 2002: An examination of the sensitivity of numerically simulated wildfires to low-level atmospheric stability and moisture, and the consequences for the Haines Index. *International Journal of Wildland Fire* 11:213–232. doi:10.1071/WF02006

Jenkins MA, 2004: Investigating the Haines Index using parcel model theory. *International Journal of Wildland Fire* 13:297–309. doi:10.1071/WF03055

Johannessen, C. L., W. A. Davenport, A. Millet, and S. McWilliams. 1971: The vegetation of the Willamette Valley. *Annals of the Association of American Geographers* 61: 286-302.

Kistler, R., E. Kalnay, W. Collins, S. Saha, G. White, J. Woollen, M. Chelliah, W. Ebisuzaki, M. Kanamitsu, V. Kousky, H. van den Dool, R. Jenne, and M. Fiorino, 2001: The NCEP-NCAR 50-year reanalysis: Monthly means CD-ROM and documentation. *Bulletin of the American Meteorological Society*, 82:247-267.

Kuchler, A.W. 1964: Potential natural vegetation of the conterminous United States. Amer. Geogr. Soc. Special Publ. 36.

Lugo, A.E., Brown, S., Dodson, R., Smith, T.M. and Shugart, H.H. 2000: The Holdridge life zones of the conterminous United States in relation to ecosystem mapping. *Journal of Biogeography* 26:1025-1038.

McCabe, G.J., and M.D. Dettinger, 1999: Decadal variations in the strength of ENSO teleconnections with precipitation in the western United States. *International Journal of Climatology* 19: 1399-1410.

McKee, T.B., N.J. Doesken and J. Kleist, 1993: The relationship of drought frequency and duration to time scales. Preprints, Eighth Conf. on Applied Climatology, Anaheim, CA, *Amer. Meteor. Soc*., 179-184.

Minore, D., 1979: Comparative autecological characteristics of northwestern tree species. USDA, Forest Service, Gen. Tech. Rept. GTR-PNW-87, Portland, Oregon.

Mitchell, T. D., T. R. Carter, P. D. Jones, M. Hulme, and M. New, 2003: A comprehensive set of high-resolution grids of monthly climate for Europe and the globe: the observed record (1901-2000) and 16 scenarios (2001-2100). *Journal of Climate*, submitted.

Pyne, S.J., P.L. Andrews, and R.D. Laven, 1996: Introduction to Wildland Fire. John Wiley and Sons, New York, NY. 769 pp

Romme WH and DG Despain, 1989: Historical perspective on the Yellowstone fires of 1988. *BioScience* 39: 695–99

Rorig, M.L. and S.A. Ferguson, 1999: Characteristics of lightning and wildland fire ignitions in the Pacific Northwest. *J. of Applied Meteorology*, 38:1565-1575.

Rorig, M.L. and S.A. Ferguson, 2002: The 2000 fire season: Lightening caused fires. *J. of Applied Meteorology*, 41:786-791.

Rothermel, R.C., 1972: A mathematical model for predicting fire spread in wildland fuels. USDA For. Serv. Res. Pap. INT-115. Intermountain Forest and Range Expt. Sta., Ogden UT. 40 p

Rothermel, R.C., 1991: Predicting behaviour of 1988 Yellowstone fires: projections versus reality. *International Journal of Wildland Fire*, 1:1-10.

Schmidt, Kirsten M.; Menakis, James P.; Hardy, Colin C.; Hann, Wendel J.; Bunnell, David L. 2002. Development of coarse-scale spatial data for wildland fire and fuel management. General Technical Report RMRS-GTR-87. Fort Collins, CO: U.S. Department of Agriculture, Forest Service, Rocky Mountain Research Station, 41 p + CD.

Simard, A.J., D.A. Haines, and W.A. Main (1985). Relations between El Niño /Southern Oscillation anomalies and wildland fire activity in the United States. *Agricultural and Forest Meteorology* 36:93-104.

Sitch, S., B. Smith, I.C. Prentice, A. Arneth, A. Bondeau, W. Cramer, J.O. Kaplan, S. Levis, W. Lutch, M.T. Sykes, K. Thorniche, and S. Venevsky, 2003: Evaluation of ecosystem dynamics, platn geography and terrestrial carbon cycling in the LPJ dynamic global vegetation model. *Global Change Biology*, 9:161-1

Skinner, W.R., Stocks, B.J., Martell, D.L., Bonsal, B., and Shabbar, R., 1999: The association between circulation anomalies in the mid-troposphere and area burned by wildland fire in Canada. *Theoretical and Applied Climatology* 63: 89-105.

Smith, B., I. C. Prentice, and M. T. Sykes, 2001: Representation of vegetation dynamics in the modelling of terrestrial ecosystems: Comparing two contrasting approaches within European climate space, *Global Ecol. and Biogeogr*., 10:621– 638.

Snyder, R., D. Spano, P. Duce, L. Xu, and K.T. Paw U,, 2003: Using surface renewal analysis to develop a fire risk index. 5th Sympsium on Fire and Forest Meteorology, American Meteorological Society, paper P3.2.

Swetnam, T. W. and J. L. Betancourt, 1998: Mesoscale disturbance and ecological response to decadal climatic variability in the American Southwest. *Journal of Climate*, 11:3128-3147.

Thonicke, K., S. Venevsky, S. Sitch, and W. Cramer 2001: The role of fire distrubance for global vegetation dynamics: coupling fire into a Dynamic Vegetation Model. *Global Ecology and Biogeography*, 10:661-677.

Thompson, S. L. and D. Pollard, 1995: A global climate model (GENESIS) with a land-surface transfer scheme (LSX). Part I: present climate simulation. *Journal of Climate*, 8:732-761.

Thorson, T.D., S.A. Bryce, D.A. Lammers, A.J. Woods, J.M. Omernik, J. Kagan, D.E. Pater, D.E., and J.A. Comstock, 2002: Ecoregions of Oregon. (2 sided color poster with map, descriptive text, summary tables, and photographs). U.S. Geological Survey, Reston, VA. Scale 1:1,350,000.

Westerling, A. L., A. Gershunov, T. J. Brown, D. R. Cayan, and M. D. Dettinger, 2003: Climate and wildfire in the western United States. *Bulletin of the American Meteorological Society*, 84:595-604.